Article

Cell Metabolism

Warmth Prevents Bone Loss Through the Gut Microbiota

Graphical Abstract

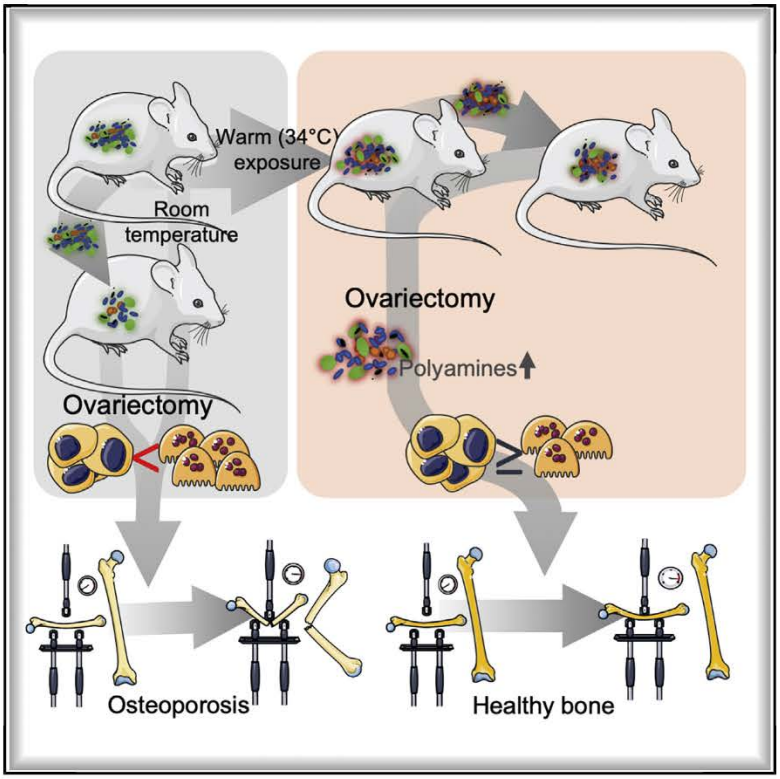

Authors

Claire Chevalier, Silas Kieser, Melis Çolakoğlu, ..., Andrew Macpherson, Nicolas Bonnet, Mirko Trajkovski

Correspondence

mirko.trajkovski@unige.ch

In Brief

Osteoporosis is a disease manifested by bone loss and increased fracture risk. Chevalier et al. observe an inverse correlation between average environmental temperature and incidence of hip fractures in humans, and they demonstrate that warmth exposure prevents osteoporosis in mice, partially through changes in the gut microbiota and an increase in polyamine biosynthesis.

Highlights

- Warm exposure improves bone strength in adulthood and prevents osteoporosis in mice
- Human meta-analyses show inverse correlation between hip fractures and temperature
- Transplantation of warm-adapted microbiota prevents bone loss
- Warmth enhances production of polyamines that increase bone strength

Chevalier et al., 2020, Cell Metabolism 32, 575–590
October 6, 2020
https://doi.org/10.1016/j.cmet.2020.08.012

CellPress

Cell Metabolism

CellPress

Article

Warmth Prevents Bone Loss Through the Gut Microbiota

Claire Chevalier,[1,2] Silas Kieser,[1,2] Melis Çolakoğlu,[1,2] Noushin Hadadi,[1,2] Julia Brun,[3] Dorothée Rigo,[1,2] Nicolas Suárez-Zamorano,[1,2] Martina Spiljar,[1,2] Salvatore Fabbiano,[1,2] Björn Busse,[4] Julijana Ivanišević,[5] Andrew Macpherson,[6] Nicolas Bonnet,[2,7,8] and Mirko Trajkovski[1,2,9,*]

[1]Department of Cell Physiology and Metabolism, Centre Médical Universitaire (CMU), Faculty of Medicine, University of Geneva, 1211 Geneva, Switzerland

[2]Diabetes Center, Faculty of Medicine, University of Geneva, 1211 Geneva, Switzerland

[3]Division of Bone Diseases, Geneva University Hospitals, 1211 Geneva, Switzerland

[4]Institute for Osteology and Biomechanics, University Clinics Hamburg, 22529 Hamburg, Germany

[5]Metabolomics Unit, Faculty of Biology and Medicine, University of Lausanne, 1005 Lausanne, Switzerland

[6]Department for Biomedical Research, University of Bern, University Clinics for Visceral Surgery and Medicine, Inselspital, Bern University Hospitals, 3008 Bern, Switzerland

[7]Division of Bone Diseases, Geneva University Hospitals, 1211 Geneva, Switzerland

[8]Present address: Nestlé Research, Innovation EPFL Park, 1015 Lausanne, Switzerland

[9]Lead Contact

*Correspondence: mirko.trajkovski@unige.ch

https://doi.org/10.1016/j.cmet.2020.08.012

SUMMARY

Osteoporosis is the most prevalent metabolic bone disease, characterized by low bone mass and microarchitectural deterioration. Here, we show that warmth exposure (34°C) protects against ovariectomy-induced bone loss by increasing trabecular bone volume, connectivity density, and thickness, leading to improved biomechanical bone strength in adult female, as well as in young male mice. Transplantation of the warm-adapted microbiota phenocopies the warmth-induced bone effects. Both warmth and warm microbiota transplantation revert the ovariectomy-induced transcriptomics changes of the tibia and increase periosteal bone formation. Combinatorial metagenomics/metabolomics analysis shows that warmth enhances bacterial polyamine biosynthesis, resulting in higher total polyamine levels *in vivo*. Spermine and spermidine supplementation increases bone strength, while inhibiting polyamine biosynthesis *in vivo* limits the beneficial warmth effects on the bone. Our data suggest warmth exposure as a potential treatment option for osteoporosis while providing a mechanistic framework for its benefits in bone disease.

INTRODUCTION

External temperature is an environmental parameter that affects various aspects of physiology and requires constant adaptation by living organisms to its fluctuations. To dissipate heat, rodents increase skin vasodilation at specific locations where the surface-to-body ratio is high. They also adapt to increased temperatures partly by enlarging the tail and ear length/surface (Meyer et al., 2017; Alhilli and Wright, 1983; Ashoub, 1958; Harland, 1960), allowing further heat dissipation. Warmth exposure also has effects on development, for example, promoting femur growth (Romsos et al., 1985; Serrat et al., 2008) and favoring denser trabecular and cortical microarchitecture (Iwaniec et al., 2016). Unilateral heating of the limb from weaning is associated with elongation of the extremities on the heat-exposed side only (Serrat et al., 2015), and chondrocyte proliferation *in vitro* is higher at warmer incubation temperatures (Serrat et al., 2008; Serrat, 2014).

Osteoporosis is the most prevalent metabolic bone disease, characterized by low bone mass and microarchitectural deterioration (Sözen et al., 2017), leading to weaker bones and increased fracture risk. Bone remodeling is enabled by the coordinated action of the two major type of cells present in the bone: osteoblasts, which are responsible for bone formation and osteoclasts, which are involved in bone resorption. The most common type of primary osteoporosis occurs as a result of post-menopausal estrogen deficiency (Reginster and Burlet, 2006), and as such, it is exceedingly common in aging females but can also occur in men. Whether heat administration post-development and during late adulthood in healthy, or during osteoporotic states, can affect bone health, remodeling, and physiology is unknown.

The intestinal flora has emerged as an important regulator of host physiology, including the bone (Li et al., 2019; Hsu and Pacifici, 2018; Jones et al., 2017; Ohlsson and Sjögren, 2015, 2018; Parvaneh et al., 2014; Sjögren et al., 2012). We (Chevalier et al., 2015) and others (Ziętak et al., 2016) have previously shown that the host adaptation to cold is in part mediated by alterations of the gut microbiota composition. However, it is not clear whether

elevated environmental temperature can affect the microbiota composition. It is also not known whether such alterations would have any effect on bone morphology and strength.

In this study, we show that warmth exposure applied at later stages of development improves bone microarchitecture and strength during healthy conditions. We further demonstrate that this phenomenon can be used in pathological conditions, where it prevents the deleterious effect of estrogen depletion in a mouse model of osteoporosis. These osteological improvements are mediated by warm temperature-induced alterations of the gut microbiota composition and are sufficient to prevent bone loss, indicating an existence of a signaling axis between warmth exposure and the bone that is mediated by the microbiota. In terms of possible translation, we performed human metadata analysis and found an inverse correlation between the incidence of osteoporotic hip fractures and external temperature that is independent of vitamin D and calcium levels. Mechanistically, through a combinatorial metagenomic, targeted metabolomic, and functional approach, we show that the warm-adapted microbiota has a higher potency to produce polyamines; in particular, acetylated spermidine and putrescine. Polyamine biosynthesis inhibition limits the benefits of warmth exposure, while polyamine supplementation mimics the effects of warmth *in vivo* in the mouse osteoporosis model. Our data suggest warmth exposure as a potential treatment option for the prevention of osteoporosis, while providing a mechanistic understanding of the role of a microbiota-host interaction during warmth exposure and bone disease.

RESULTS

Warmth Exposure Improves Bone Strength in Adulthood

Aging leads to a decrease in bone strength and mass and alterations in the microarchitecture (Boskey and Coleman, 2010; Demontiero et al., 2012; Mosekilde, 2000), which can increase the incidence of fracture. We, therefore, evaluated the effects of warm temperature exposure on mice after their development, using females exposed for 8 weeks to 34°C starting at 16 weeks of age. This treatment led to an increase in the tail length in the older female mice (Figure S1A), and the increase was even more pronounced following 34°C exposure for 1 month when started in 8-week-old male mice (Figure S1B). This was coupled to higher tail temperature as expected, without changing the overall body temperature (Figures S1C and S1D). Exposure to 34°C of the older females led to an increase in the trabecular bone volume (BV) versus total tibia volume ratio (BV/total volume [TV]), the connectivity density of the tibias (Figures 1A–1F), and in the BV/TV of the caudal vertebra (Figure 1G), without affecting the cortical bone of the tibias (Figures 1H–1J), indicating a positive effect of warmth exposure on the trabecular bone.

These structural changes were also reflected at a biomechanical level. A three-point bending test in the femur highlighted the improvements in the yield point (Figure 1K) above which mechanical force causes permanent damage to the bone structure and in the ultimate force (Figure 1L) that reflects the general integrity of the bone. No differences were detected in the elastic energy, energy to fracture, or the Young's modulus (Figures 1M–1O). Exposure to 34°C reduced the food intake by 25% (Figure S1E), consistent with slowing of the overall metabolism and reduced activity at elevated temperatures (Kaiyala et al., 2012) (Figures S1E and S1F). As lowered food intake affects the bone mass (Devlin et al., 2010; Hamrick et al., 2008) and reduces body weight at room temperature (RT) (Fabbiano et al., 2016), but not during warmth exposure (Figure S1F), we compared the effects of warmth exposure to a pair-fed set of animals kept at RT. Warmth exposure led to elevated trabecular BV/TV (Figure S1G) and higher cortical BV and width (Figures S1H–S1J) compared with the pair-fed controls. This was coupled to a marked improvement of the biomechanical resistance that was independent of the food intake (Figures S1K–S1O). In addition, the warmth exposure also led to elongated femurs in comparison to the pair-fed RT-housed controls (Figure S1P). These data show that warmth exposure exerts beneficial effects on the biomechanical bone parameters in mice during adulthood and that these effects are unrelated to the decreased food intake.

Warmth Exposure Correlates with Reduced Fracture Incidence in Humans and Prevents Experimentally Induced Bone Loss in Mice

We next investigated if the warmth exposure could have protective effects on bone loss. To address the potential relevance of the temperature on the osteoporosis-related fractures in humans, we performed human metadata analysis on the incidence of hip fractures per capita and country worldwide (Cauley et al., 2014; Wahl et al., 2012; Balk et al., 2017) and found a positive correlation between the fractures and the latitude (Figures 2A and S2A). Conversely, there was a negative correlation between the average temperature and hip fracture incidence both in women and in the total population (Figures 2B and S2B). Partial correlation analysis (with the effect of the vitamin D removed) showed that the temperature and latitude effect on the hip fracture incidence are independent of vitamin D (Figures S2C–S2G). Similarly, correcting for the calcium intake did not influence the effect of the temperature and latitude on the hip fracture incidences (Figures S2H and S2I). Instead, when correcting for temperature, the association between latitude and the hip fracture was largely eliminated (Figure S2J).

To directly test if warmer temperatures may exert protective effect on bone loss, we surgically ovariectomized 16-week-old mice, which is the most commonly used model for primary osteoporosis, and exposed them to 34°C or RT for 8 weeks (Ova34°C or OvaRT, respectively), using sham-operated mice as controls (Sham34°C or ShamRT). Warmth exposure lowered the food intake as expected, and this was unaffected by the oophorectomy (Figure S2K). Strikingly, warmth exposure prevented the trabecular BV/TV loss caused by ovariectomy (Figure 2C), as assessed by computed tomography (CT) and normalized to body weight (Figure S2L). This was consistent with the increase in the trabeculae number, the trabecular thickness, and the connectivity density (Figures 2D–2H) in the Ova34°C mice, compared with the OvaRT controls. No differences were detected in the trabecular spacing and femur length (Figures 2G and S2M). The ovariectomy-induced decrease in the cortical BV and width of tibias was prevented in the Ova34°C mice to similar levels as the ShamRT controls (Figures 2I–2K). This phenomenon was not restricted to long bones as we found that the decrease in the BV/TV of the caudal vertebra in the Ova34°C

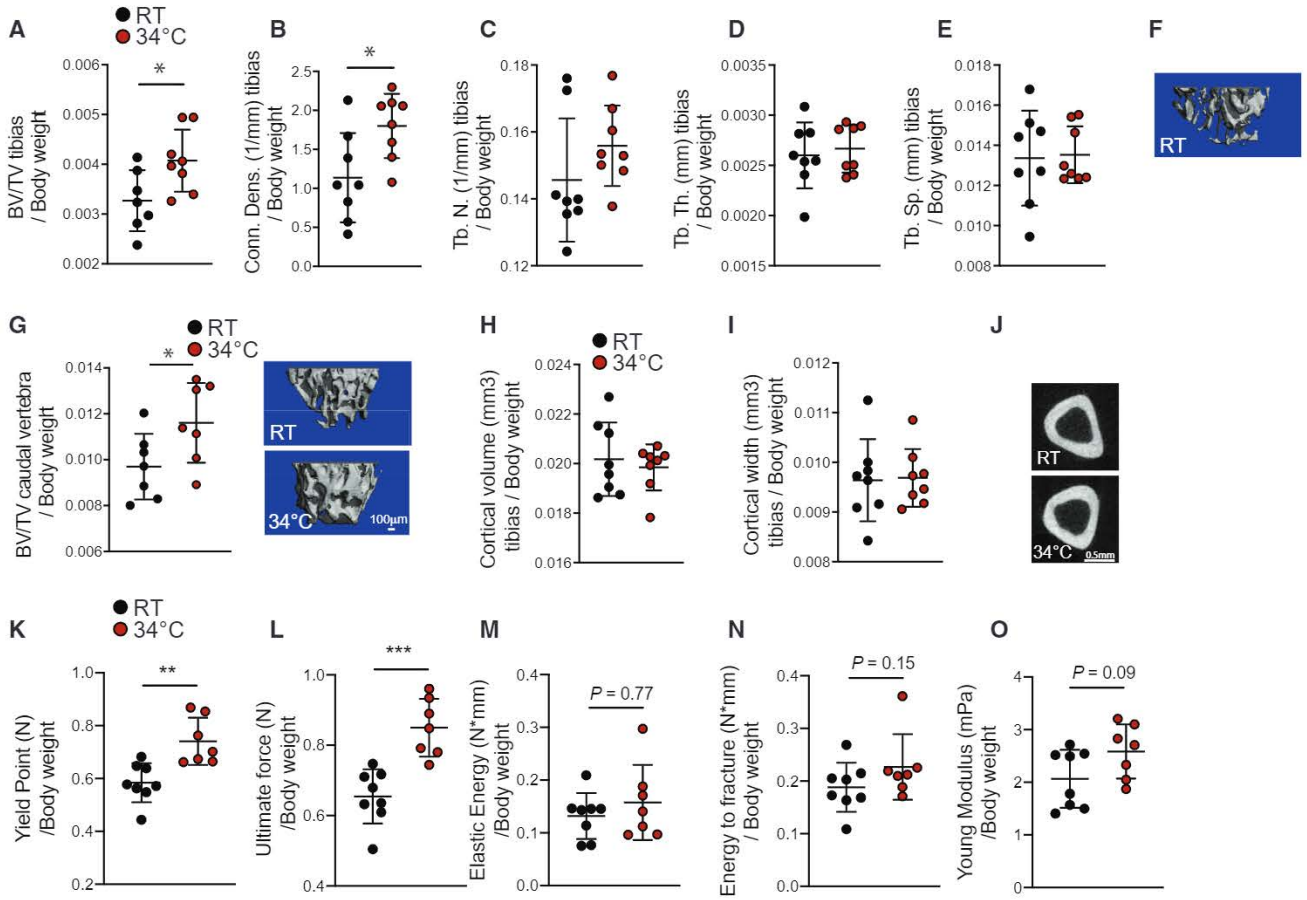

Figure 1. Warmth Exposure Improves Bone Strength during Adulthood

(A–E) Trabecular bone microarchitecture of tibias showing BV/TV (A), connectivity density (Conn. Dens) (B), number of trabeculae (Tb. N) (C), trabecular thickness (Tb.Th.) (D), and trabecular separation (Tb.Sp) (E) of 24-week-old female mice exposed to 34°C for 2 months prior to sacrifice and their RT controls (n = 8 per group), all normalized to body weight.

(F) Representative reconstruction of trabecular bone used for the calculations in (A)–(F). Scale bar, 100 μm. Each trabecular reconstruction was done by scanning and compiling 262 sections from the beginning of the growth plate to the midshaft in each mouse using n = 8 per group.

(G and H) Cortical BV (G) and width (H) of mice as in (A), measured in midshaft of the tibias and normalized to body weight. (G) Right: representative reconstruction (each consisting of 262 sections, n = 8 per group) of trabecular bone used for calculation. Scale bar, 100 μm.

(I) Representative cortical section (from 62 sections per bone of each mouse of n = 8 per group). Scale bar, 0.5 mm.

(J) BV/TV (left), measured in the caudal vertebra (CA2) (normalized to body weight) of mice as in (A).

(K–O) Biomechanical analysis of femur from mice as in (A) using a three-point bending test. The parameters measured include the yield point (K), the ultimate force (L), the elastic energy (M), the energy to fracture (N), and the Young's modulus (O) and normalized to their respective body weight.

Data are shown as mean ± SD (n = 8 per group). Significance (p value) is calculated using Mann-Whitney t test, *p < 0.05; **p < 0.01; ***p < 0.001.

mice was ameliorated to the levels seen in the ShamRT controls (Figure 2L). These structural improvements were accompanied by a reduced fragility of the bones in the Ova34°C mice, as shown by the biomechanical measurements during the three-point bending test (Figures 2M–2Q), as they showed similar reads for all the mechanical properties as the ShamRT controls, except for the elastic energy.

Warmth Exposure Alters the Microbiota Composition

Recent evidence suggest an interaction between the gut microbiota and bone metabolism (Li et al., 2019; Ohlsson and Sjögren, 2015; Hsu and Pacifici, 2018). To investigate whether warmth exposure can alter the microbiota composition, we performed 16S ribosomal DNA analysis of microbiota in cecum and feces from 24-week-old female mice that have been exposed to 34°C for 8 weeks. Among the 892 identified operational taxonomic units (OTUs), 81 were differently abundant ($p \leq 0.05$) in warmth- versus RT-treated animals. Principal component analysis (PCA) of all the microbiomes showed segregation between the two groups (Figure 3A). Despite the reduced richness of the gut flora after warmth exposure, the Shannon diversity was higher (Figures 3B and 3C), indicating a more even distribution in abundance of the bacterial species after warmth exposure. This observation was further supported by the family relative abundance (Figure 3D), where the predominance of the *Muribaculaceae* family was dampened in the warm-adapted microbiota. The hierarchical clustering of the samples associated with a heatmap confirmed the clustering of the microbiota

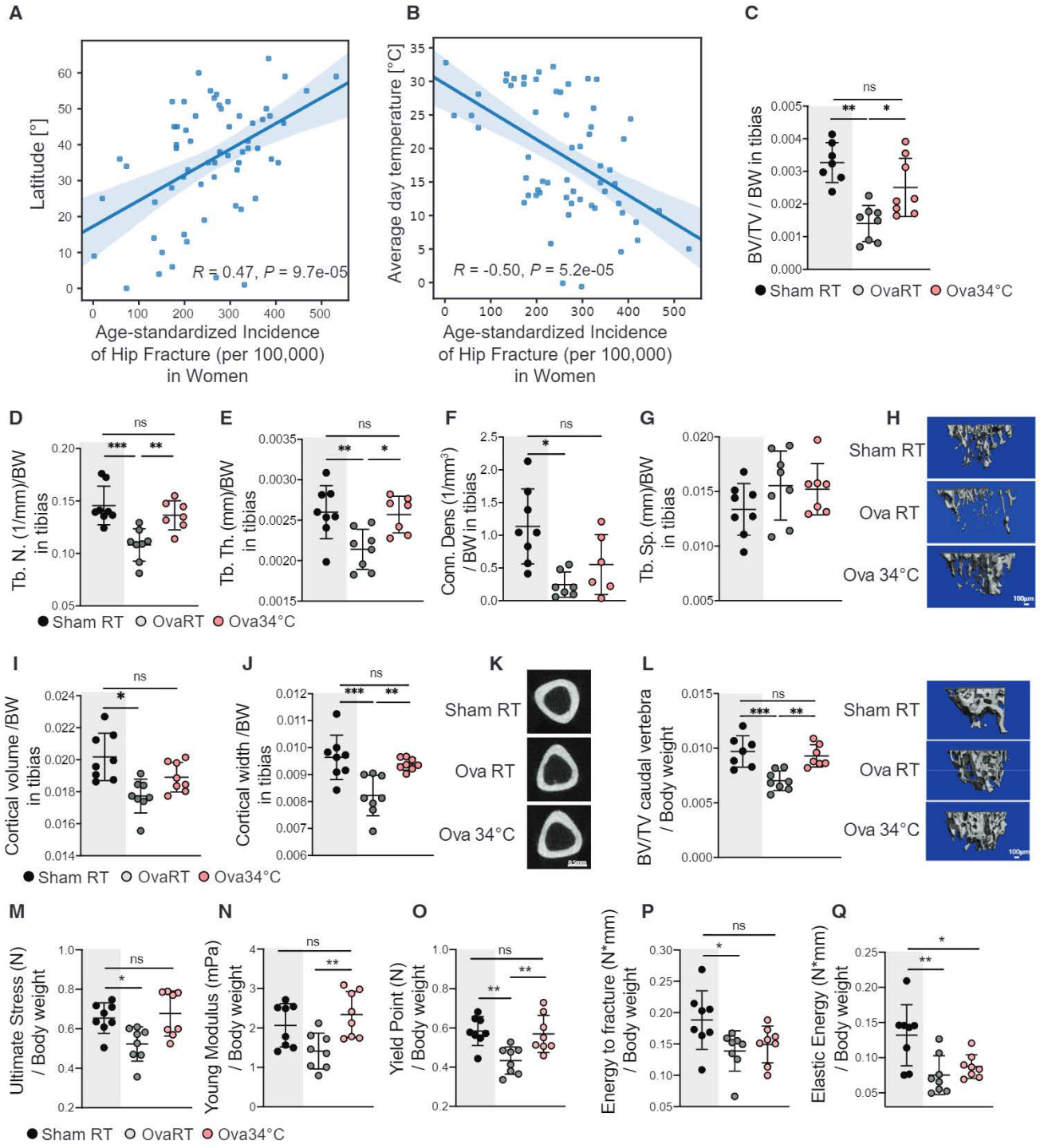

Figure 2. Warmth Exposure Protects against Osteoporosis

(A and B) Metadata analysis showing age-standardized correlation between hip fracture incidence (per 100,000 inhabitants) in women per country versus the latitude of the country's capitals (A) or versus the country's average day temperature (B).

(C–H) Trabecular bone microarchitecture of tibias in female mice that were ovariectomized, or sham-operated at 16 weeks of age, and then exposed to 34°C for 2 months (Ova34°C or Sham34°C, respectively), or kept at RT (OvaRT or ShamRT). BV/TV (C), the number of trabeculae (Tb. N) (D), the trabecular thickness (Tb.Th.) (E), the connectivity density (Conn. Dens) (F), and the trabecular separation (Tb.Sp) (G) from the mice as in (C) at the end of the warm exposure, normalized to their respective body weight. (H) Representative reconstruction (each consisting of 262 sections, n = 8 per group) of trabecular bone used for calculations. Scale bar, 100 μm.

(I and J) Cortical BV (I) and width (J) of mice as in (C) measured in the midshaft of the tibias and normalized to the body weight.

(legend continued on next page)

following warmth exposure, as well as the broad change in the microbial composition (Figure 3E). At a genus level, we observed a warm microbiota signature associated with an increase of the genera *Turicibacter*, *Ruminiclostridium_6*, *Akkermansia*, *Rhodospirillales*, *Clostridium_sensus_stricto_1*, and *Parabacteroides*, and a reduction of *GCA.900066575*, *Butyricicoccus*, *Peptococcaceae*, *or Ruminiclostridium* (Figures 3F and S3A). Curiously, despite the reduction of *Muribaculum* at the genus level, several of its OTUs were among the most elevated following warmth exposure, pointing to an extreme variability of the growth behavior within this genus (Figures 3G and S3B). *Akkermansia muciniphila* showed a strong increase in abundance after warmth exposure. Interestingly, this same species was strongly suppressed after cold exposure (Chevalier et al., 2015; Ziętak et al., 2016), suggesting that *Akkermansia muciniphila* is consistently affected by the environmental temperature.

To confirm the effect of the warm housing temperature in shaping the microbiota, we performed similar analysis in mice of different age and sex. Similar to the effect in the older females, 12-week-old male mice that were exposed to 34°C for 4 weeks showed altered microbiota composition as shown by PCA (Figure S3C), but without showing differences in the Shannon diversity or Richness (Figure S3D). The family abundance bar chart analysis revealed similar changes between the older females and the younger males despite the difference in the treatment length, with overall increase in the *Akkermansiaceae* and reduction of the *Muribaculaceae* family (Figure S3E). Similar to the most altered OTUs in the older females, *Muribaculaceae OTU2594*, *Clostridium_stricto_sensus_1_OTU2703*, and *Lactobacillus_otu2644* were more abundant (Figure S3F) in the microbiota of the warmth-exposed male mice than that of the RT controls. While the estrogen depletion caused changes in gut microbiota population (Figures S3G–S3H) (Markle et al., 2013; Cox-York et al., 2015; Kaliannan et al., 2018), the effects of warmth exposure on the microbiota composition were maintained after ovariectomy, with an increase in the *Akkermansiaceae* and reduction in the *Muribaculaceae* family. To further investigate the particular signature of the warmth exposure in changing the microbiota, we directly compared the warm-induced changes in the above three conditions: older female, young male, and ovariectomized mice. By plotting the PCAs, we observed a consistent shift in the microbiota composition selected by the PC2 (Figure S3H). Additional comparison of the 3 groups selected for consistent changes and a p value < 0.05, further supported these observations, and provided a signature of the warmth exposure on the microbiota composition with increase of *Muribaculaceae otu2594*, *Muribaculaceae otu2618*, *Lactobacillus otu2644*, *Clotridium_stricto_sensu_1_otu2703*, and *Lachnospiraceae otu2806* (Figure S3I). Accordingly, warmth exposure leads to robust and consistent changes in the gut microbiota composition that is independent of age, sex, or hormonal status.

Transplantation of Warm-Adapted Microbiota Prevents Bone Loss

To uncover whether the microbiota impacts the bone parameters during warmth exposure, we first eliminated the microbiota using antibiotics. Microbiota depletion abolished the warmth-induced increase in femur strength in 23-week-old female mice (Figures S3J–S3N) and limited the warmth-mediated increase in trabecular BV and connectivity density of the tibia (Figures S3O–S3S). Similarly, warmth exposure did not alter the cortical bone in the microbiota-depleted mice (Figures S3T–S3V). To directly test the importance of the warm-adapted microbiota in a pathological context, we used mice that were ovariectomized at 16 weeks of age and recurrently transplanted with fecal microbiota of either warmth-exposed or RT-kept mice (OvaTransp34°C or OvaTranspRT; Figure S4A). Both microbiota-transplanted groups of mice were maintained at RT to isolate the microbiota effect. The PCA of the transplanted mice suggested microbiota similarities to the respective donors (Figure S4B). These observations were supported by the conserved microbial signature described earlier, including changes in the *Lactobacillus otu2644* and *Muribaculaceae otu2596*, which were maintained in the transplanted groups (Figure S4C).

The recurrent microbiota transplantation did not affect the body weight gain, nor did it change the food intake (Figures S4D and S4E). However, tibia measurements before and after the transplantation showed higher BV in the OvaTransp34°C than that of the OvaTranspRT mice (Figures 4A–4C and 4E). The increased tibia BV was associated with greater connectivity density delta before versus after microbiota transplantation (Figure 4D) in the OvaTransp34°C compared with the delta in the OvaTranspRT without affecting the trabecular thickness, trabeculae space and number (Figure S4F), and the cortical BV and width (Figures 4F–4H). The bone strength was improved at different levels during the three-point bending test on the femurs (Figures 4I–4M), collectively indicating that the protective effect observed during warmth exposure on the bone loss outcome is in part phenocopied by the warm microbiota transplantation.

We also investigated whether microbiota transplantation could have an effect in non-pathological conditions, using male germ-free (GF) mice transplanted with microbiota from male donors that were exposed to warmth for 4 weeks, or kept at RT. The PCA of the microbiota from the transplanted GF mice revealed differences between the groups (Figures S4G and S4H; data not shown). Fecal warm microbiota transplantation of the young male GF mice led to higher cortical BV and width (Figures S4I and S4J), despite these measurements being done only 20 days after the transplantation, without affecting the femur length (Figure S4L). Warm microbiota transplantation in the GF mice led to a slight improvement in the bone strength parameters compared with the RT-microbiota-transplanted controls (Figure S4K). These data show that warm-adapted microbiota

(K) Representative cortical sections from each group (from 62 sections per bone of each mouse of n = 8 per group). Scale bar, 0.5 mm.
(L) Trabecular BV/TV, measured in the caudal vertebra (CA2) (normalized to body weight) of mice as in (C). Right: representative reconstruction (each consisting of 262 sections, n = 8 per group) of a vertebra used for calculation. Scale bar, 100 μm.
(M–Q) Biomechanical analysis of femur from mice as in (C) showing ultimate stress (M), Young's modulus (N), yield point (O), energy to fracture (P), and elastic energy (Q), all normalized to the body weight.
Data are shown as mean ± SD (n = 8 per group). Significance (p value) is calculated using Mann-Whitney t test, *$p < 0.05$; **$p < 0.01$; ***$p < 0.001$. Sham RT mice (as shown in Figure 1) are shadowed in gray.

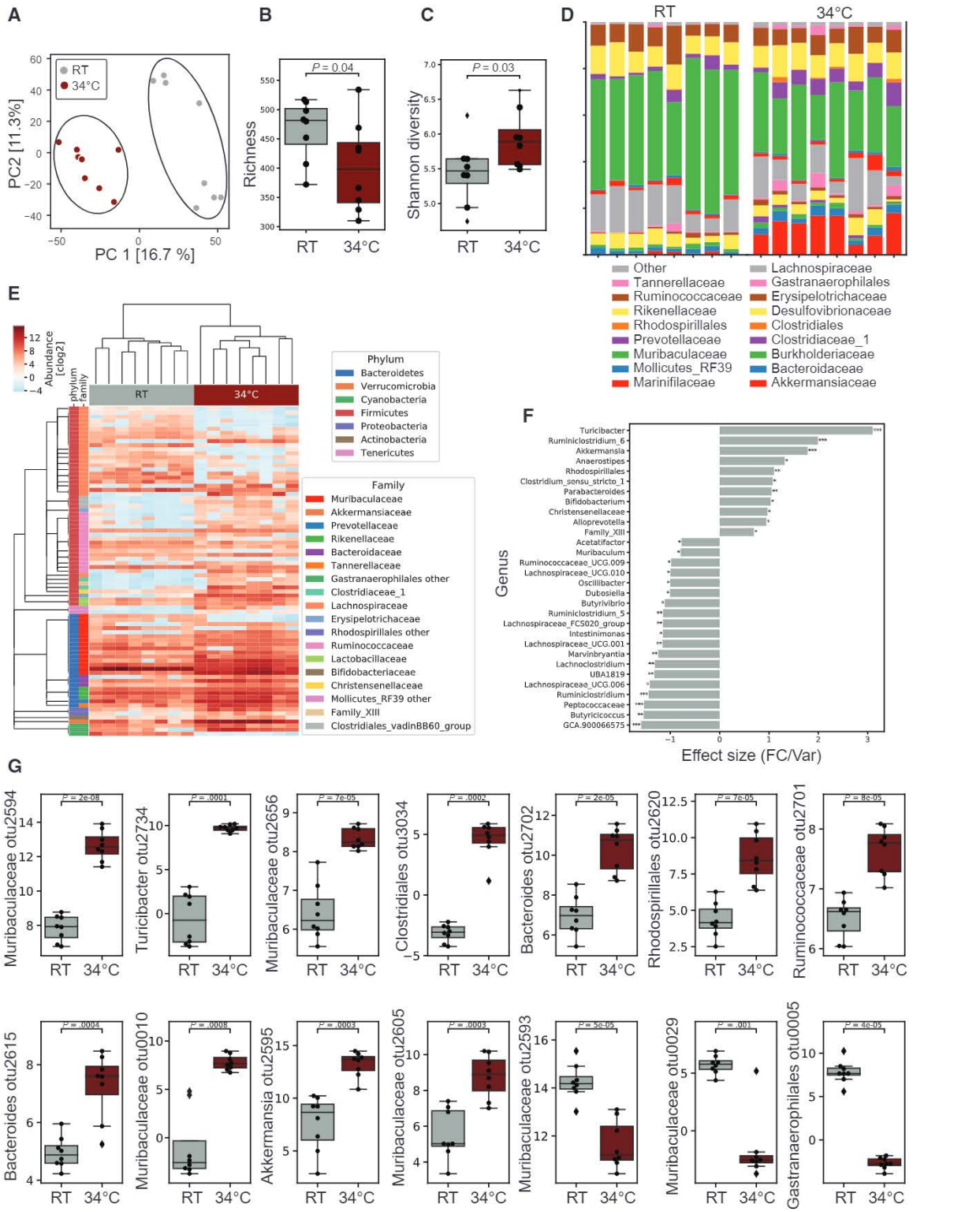

Figure 3. Warmth Exposure Changes the Gut Microbiota Composition

(A) PCA of 16S rDNA sequencing of fecal microbiota from 24-week-old female mice exposed for 2 months to 34°C or kept at RT. Each dot represents a fecal microbiota from one mouse. The analysis is based on the centric log2 ratio (CLR).

(B and C) Estimated richness (B) and Shannon diversity (C) of microbiota samples as in (A).

(D) Bar chart of the relative microbiome abundance at family level from mice as in (A).

(legend continued on next page)

transplantation improves bone strength and physiology, with the effect being more pronounced in pathological conditions.

Warmth Exposure and Warm Microbiota Ameliorate the Ovariectomy-Induced Transcriptional Bone Remodeling

To gain insights into the magnitude and mechanisms of the bone remodeling, we performed RNA sequencing on tibias from ovariectomized and sham-operated mice exposed to 34°C and their RT controls, as well as from the ovariectomized microbiota-transplanted mice. Ovariectomy-induced severe transcriptional alterations, which were markedly reduced when the ovariectomized mice were kept at 34°C (Figures 5A and 5B). Specifically, to dissect the effect of warmth on the ovariectomy-induced transcriptional alterations, we selected the deregulated genes ($|\log_2FC| > 1$ in OvaRT versus ShamRT, and log count per million [CPM] > 0) and compared them to the changes in Ova34°C versus ShamRT. Strikingly, warmth exposure reduced the ovariectomy-induced transcriptomics changes in 90.5% of the genes partially or completely (93.2% from the upregulated and 86.4% from the downregulated) (Figure 5C), demonstrating that warmth exposure exerts a major protective effect on the transcriptional bone remodeling induced by estrogen deficiency. Reactome pathway analysis between ovariectomized mice at RT or at 34°C indicated differences in the collagen biosynthesis and degradation, associated with extracellular matrix reorganization, suggesting that warmth exposure leads to alterations in the bone remodeling pathways at the transcriptional level (Figure 5D). Comparative analysis suggested overlap between the reactomes of ovariectomized and control non-ovariectomized mice kept at 34°C when compared with their respective RT controls (Figures 5I and S5A–S5C). Specifically, out of 21 deregulated pathways between ShamRT versus 34°C, 20 pathways (95%) were found altered by warmth exposure in the ovariectomized mice (OvaRT versus 34°C).

Transplantation of the ovariectomized mice with the warm-adapted microbiota (OvaTransp34°C) also induced transcriptional alterations (FDR < 0.01 and $|\log_2FC| > 1$) in bone when compared with the RT-microbiota-transplanted controls (OvaTranspRT) (Figure 5E). To investigate if the warm-adapted microbiota could exert similar effect as the warm exposure on mitigating the ovariectomy-induced transcriptional deregulation, we specifically analyzed the altered genes (shown in Figure 5C) in the OvaTransp34°C mice compared with the OvaTranspRT controls. Interestingly, the ovariectomy-induced transcriptional changes were reduced or reverted in 59% of the total deregulated, and in 94% of the reduced genes (shown in green in Figure 5F), when the ovariectomized mice were transplanted with warm microbiota, similar to the direct effect of warmth exposure (Figures 5F and 5G). In the top 10 deregulated reactome pathways of the microbiota-transplanted ovariectomized mice, we observed a similar pattern to the warmth-exposure-induced changes (Figure 5H). These data indicate that warmth exposure and warm microbiota transplantation suppress the ovariectomy-induced transcriptional alterations.

Warmth and Warm Microbiota Enhance Periosteal Bone Formation

To gain further insights into the mechanisms by which warmth exposure increases bone strength, we investigated the number and activity of the cells responsible for the bone remodeling. During homeostasis, the activity of osteoblast and osteoclasts is at equilibrium. In the context of osteoporosis, the overall bone remodeling is increased, where the activity of the osteoclasts is superior to the one of the osteoblasts, leading to bone loss. We quantified the osteoblast activity by measuring the fluorescent calcein deposits within the bone during its formation between 2 injections, 7 days apart. The cortical bone in the midshaft of the femur showed a specific increase of the periosteal mineralized surface in the ovariectomized mice exposed to warmth compared with the RT-housed controls, without the endocortical surface and the trabecular bone mineralization (measured in the head of the femur) being affected (Figures 6A–6C and S5D). The increased osteoblast activity was confirmed by the higher levels of circulating osteocalcin in the warmth-exposed ovariectomized mice, but not in the sham-operated controls (Figures 6D and S5E). Consistent with warmth exposure, the specific increase in the periosteal mineral apposition rate (MAR) was observed in the ovariectomized mice receiving the warm-adapted microbiota (Figures 6E–6I and S5F), suggesting that similar mechanisms mediate the effects of warmth exposure and warm microbiota transplantation. The active osteoclast number was then quantified using Tartrate-resistant acid phosphatase (TRAP) staining on femur trabecular histological sections. No differences were observed after warmth exposure, or warm microbiota transplantation in any of the groups (Figures 6J–6L; data not shown). This was supported by the circulating CTX-1 levels as marker of bone resorption, which was neither changed by warmth in both ovariectomized and non-ovariectomized mice, nor in the warm microbiota-transplanted animals (Figures 6M and S5G). Notably, the bone remodeling effects were independent of the collagen deposition, bone mineral content, and circulating vitamin D levels, as we did not detect differences for these parameters between any of the groups (Figures S5H–S5K; data not shown). These data indicate that warmth exposure or warm microbiota transplantation shifts the balance between osteoblast activity and the number of active osteoclasts toward bone formation.

Warmth Exposure Increases Production of Polyamines that Affect Osteoblast Activity and Decrease Osteoclast Differentiation

To investigate the link between microbiota and bone during warmth, we performed a metagenomic analysis of the gut microbiota from 24-week-old female mice that were exposed for

(E) Hierarchical clustering associated with a heatmap comparing the CLRs of the OTUs selected for a $p < 0.05$ of mice as in (A). An idealized tree represents their taxonomic hierarchy down to genus level associated with bars that are color-coded for phylum and family. Each column represents one mouse.
(F) Effect size of all significantly changed genera calculated with aldex2 (FDR < 0.05) in samples from mice as in (A).
(G) CLRs representing relative abundance of the most changed OTUs (FDR < 0.01) by warm exposure in samples from mice as in (A). Boxplots represent median and quantiles; the whiskers show 1.5 inter quartile range and values outside the whisker's box are represented as diamonds.
Data are shown as mean ± SD (n = 8 per group). Significance in (F) and (G) is calculated using Welch t test, *p < 0.05; **p < 0.01; ***p < 0.001.

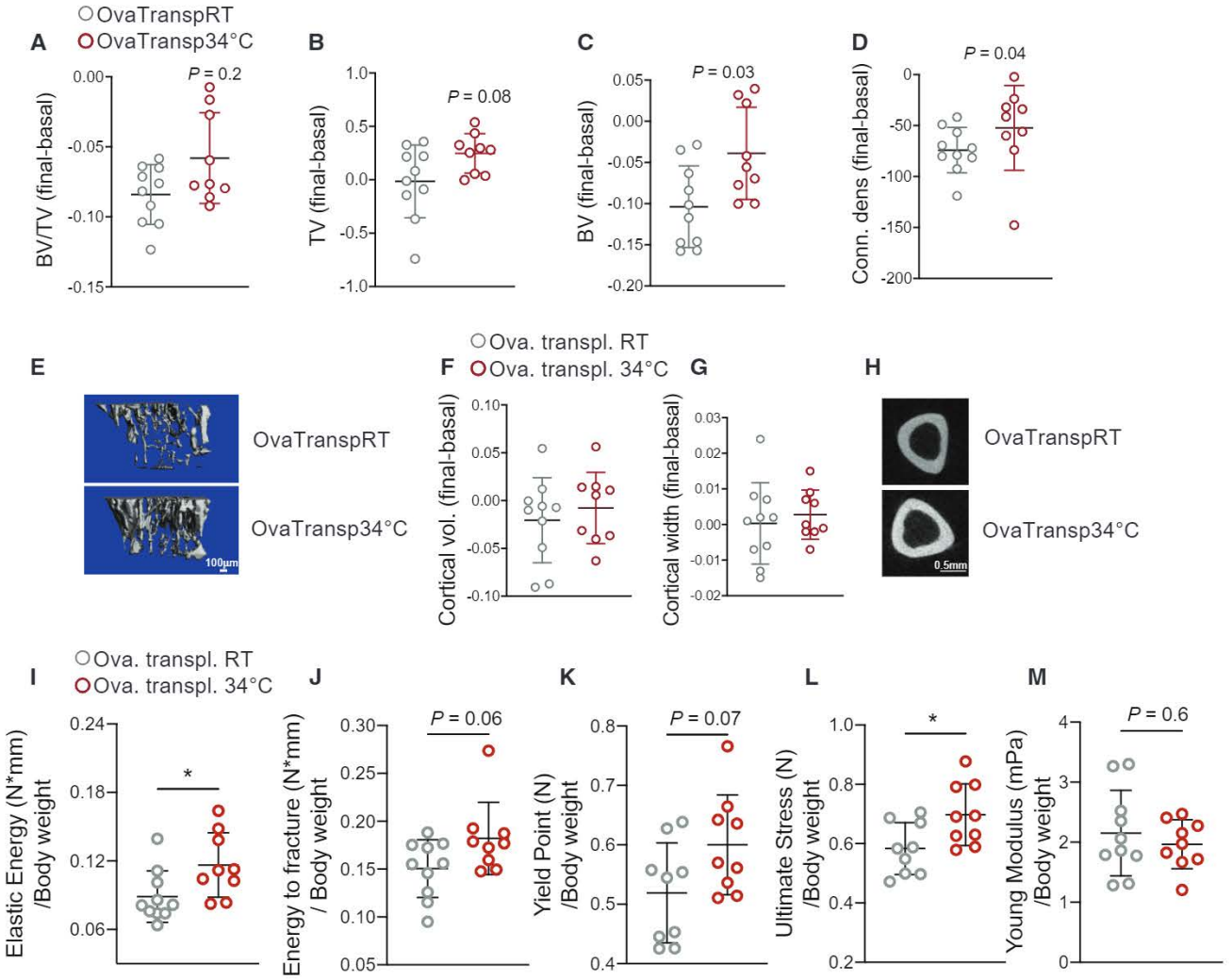

Figure 4. Warm Microbiota Transplantation Prevents Bone Loss and Improves Bone Strength

(A–D) Delta between two micro-CT measurements (day 0 and day 32 after starting the microbiota transplantation) of proximal tibias at trabecular level in 21-week-old ovariectomized, microbiota recipient female mice. The recipient mice were ovariectomized at week 16, and repetitively transplanted with fecal microbiota from 34°C exposed, or RT-kept donors (OvaTransp34°C or OvaTranspRT, respectively). The 34°C treatment of the 16-week-old female donor mice was initiated 1 month before starting the transplantations and lasted for the whole length of the experiment. BV/TV (A), BV (B), TV (C), and connectivity density (D).

(E) Representative reconstruction (each consisting of 262 sections, n = 10 per group) of trabecular bone use for the calculations. Scale bar, 100 µm.

(F–H) Cortical BV (F) and width (G) measured in midshaft of tibias from mice as in (A). (H) representative cortical section (from 62 sections per bone of each mouse of n = 10 per group). Scale bar, 0.5 mm.

(I–M) Biomechanical analysis of tibias from mice as in (A) showing elastic energy (I), energy to fracture (J), yield point (K), ultimate stress (L), and Young's modulus (M), all normalized to their body weights.

Data are shown as mean ± SD (n = 10 per group). Significance is calculated using Mann-Whitney t test, *p < 0.05; **p < 0.01; ***p < 0.001.

8 weeks to 34°C and from the RT-housed controls. Among 536 identified pathways, 134 were differentially abundant in the feces of warmth-exposed animals compared with RT controls. Within the top ten regulated pathways was the polyamine synthesis showing higher levels for the key genes responsible for polyamine production and lower levels for those involved in the polyamine degradation processes (Figures 7A, 7B, and S6A). Deeper analysis of the metagenomic data by genus suggested that expansion of *Akkermansia muciniphila* during warmth exposure, as well as the genera *Bacteroides* and *Alitsipes*, may be the main contributors to the polyamine biosynthesis (Figure S6B). Conversely, the decreased propensity of the microbiota to degrade spermine and spermidine could be attributed to the decline of the bacteria from the *Muribaculaceae* or *Lachnospirae* genera (Figure S6C). The polyamines have fast plasma turnover and rapidly reach their target tissues (Pegg, 2009). To directly test whether the metagenomic data would correlate with an actual increase in the respective polyamine metabolites, we developed an isotope dilution-based, hydrophilic interaction chromatography coupled to targeted tandem mass spectrometry (HILIC-MS/MS) method for absolute quantification of the polyamine metabolites. In agreement with the metagenomics

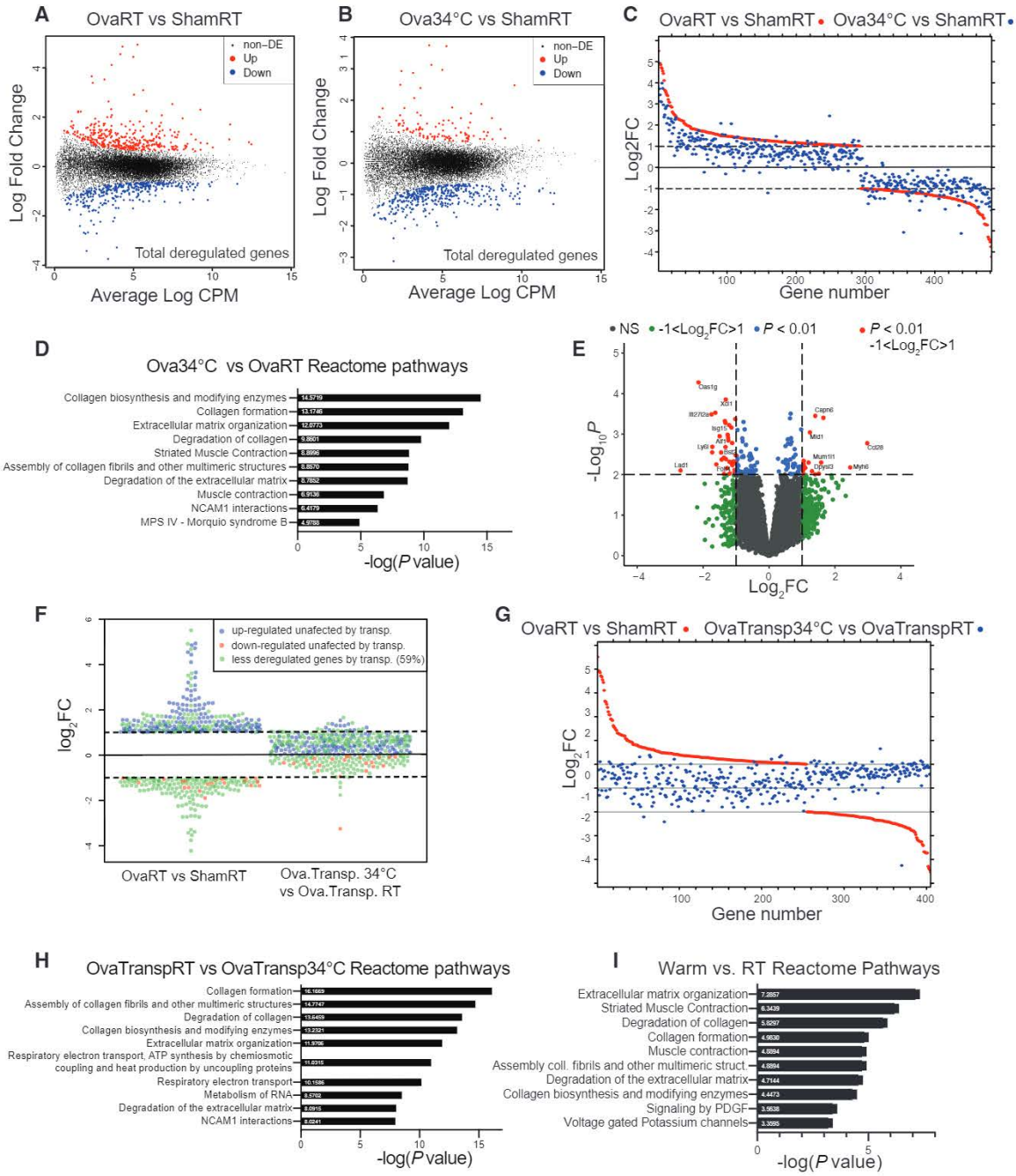

Figure 5. Warmth and Warm Microbiota Transplantation Ameliorate Ovariectomy-Induced Transcriptional Deregulation

(A) Mean-difference plot (MD-plot) of the log fold change gene expression between tibias of 24-week-old female mice that were ovariectomized or sham-operated at 16 weeks of age and then kept at RT for 2 months (OvaRT versus ShamRT, respectively) shown as average CPM. Red dots show the increased and blue show the decreased genes selected for FDR < 0.05.

(B) MD-plot of the log fold change of gene expression between tibias of 24-week-old female mice that were ovariectomized at 16 weeks of age and then kept at 34°C for 2 months (Ova34), versus ShamRT, shown as average CPM. Red dots show increased and blue show decreased genes selected for FDR < 0.05.

(C) Comparison between the log fold change of genes deregulated by ovariectomy at RT shown in red ($|\log_2 FC| > 1$; OvaRT versus ShamRT) and the same genes when exposing the ovariectomized mice at 34°C shown in blue ($|\log_2 FC| > 1$; Ova34°C versus ShamRT).

(D) Top 10 most deregulated Reactome pathways between tibias of OvaRT and Ova34°C mice.

(E) Volcano plot comparing the p value and the log fold change of gene expression between tibias of 21-week-old ovariectomized, microbiota recipient female mice (OvaTransp34°C or OvaTranspRT) as in Figures 4A–4E. Green dots, $|\log_2 FC| > 1$; blue dots, $p < 0.01$; red dots, $p < 0.01$ and $|\log_2 FC| > 1$.

(F and G) Expression analysis of the ovariectomy-altered genes ($[|\log_2 FC| > 1]$ at RT [OvaRT versus shamRT]) in tibia from OvaTransp34°C mice compared with the OvaTranspRT controls (OvaTransp34°C versus OvaTranspRT). In (F), blue and red show genes (up- or downregulated, respectively) unaltered by microbiota

(legend continued on next page)

data, the concentrations of putrescine, N1-acetylputrecine, N1-acetylspermidine, and spermine were higher in feces of the warmth-exposed animals (Figures 7C, 7D, and S6D). This was coupled to higher spermine levels in the cecum of warmth-exposed mice or elevated N1-acetylspermidine and N1N12-acetylspermidine in the warm microbiota-transplanted mice (Figures 7C, S6E, and S6F).

To test the effect of polyamines on bone cellular activity, we performed an *ex vivo* experiment with spermine and spermidine supplementation in primary osteoblast or osteoclast cultures during differentiation. Since it is difficult to correlate the *in vivo* levels with those *in vitro*, we used different concentrations in the primary cultures and assessed the outcome in a dose-response manner. Supplementation of spermine and spermidine at high (but not low) doses in osteoclasts during differentiation caused downregulation of cathepsin K (*CtsK*), TRAP 5 (*Trap5b*), and matrix metalloprotease 9 (*Mmp9*), which are markers of osteoclast activity and differentiation (Figures 7E, 7F, and S6G). The decrease in expression of the osteoclast differentiation markers was associated with a reduced number of differentiated osteoclasts measured by TRAP staining (Figures 7G and S6H). These findings are in agreement with the studies in mice that oral supplementation of spermine and spermidine in an ovariectomy-induced model of osteoporosis was sufficient to prevent bone loss, measured by %BV/TV in vertebra (Yamamoto et al., 2012). The anti-osteoclast effects of spermidine, but not spermine, were observed even when these polyamines were added after differentiation, where 24 h of spermidine supplementation was sufficient to reduce the expression level of *Ctsk* and *Trap5b* (Figures S6I and S6J). Spermine increased osteoblast expression of osteocalcin (*Ocn*) and osteoprotegerin (*Opg*) in a dose-dependent manner (Figure 7H). Similarly, elevated spermidine levels augmented osteopontin (*Opn*), osteoprotegerin (*Opg*), and receptor activator of nuclear factor kappa-B ligand (*Rankl*) expression, indicating an increased osteoblast function (Figure 7I), coupled to a decrease in the *Rankl*/*Opg* ratio that could explain the decreased osteoclastogenesis. These observations were supported by an enhanced activity of alkaline phosphatase (ALP) when spermine and spermidine were added to the osteoblasts (Figures 7J–7K). These data support the observations regarding the osteoblast function *in vivo* during warmth exposure and warm microbiota transplantation, and they demonstrate that polyamines could mediate the enhanced osteoblast activity. This increase was observed despite the slight reduction of the cell viability (lower total protein and RNA) upon spermine supplementation (Figures S6K and S6L), which may result from interaction of spermine with serum from the media, producing H_2O_2 radicals by oxidative degradation of the polyamines (Wang et al., 2018).

Finally, we directly tested the necessity of the polyamine biosynthesis in mediating the warmth-induced effects on the bone *in vivo*. Polyamine supplementation in older female mice increased the yield point, elastic energy, and energy to fracture of the femur to similar values as the warmth-exposed mice (Figures 7L–7P). Conversely, we used a polyamine biosynthesis pathway inhibitor, diaminazene acetureate (DA), which prevents formation of decarboxy-S-adenosinemethionine, a metabolite that turns into spermine and spermidine (Karvonen et al., 1985). DA also blocks spermidine and spermine acetyltransferase activity (Libby and Porter, 1992; Neidhart et al., 2014), thus, inhibiting the back conversion of spermine and spermidine toward putrescine, leading to reduced acetylspermine and acetylspermidine formation. Treating warmth-exposed older female mice with the polyamine inhibitor abolished the warmth-induced increase in the yield point and elastic energy during the three-point binding test in femur, revealing similar biomechanical parameters between the warmth-exposed, DA-treated mice and the RT-housed controls (Figures 7L–7P). Moreover, the warmth-induced increase in the trabecular BV and connectivity density of tibia were reduced in the polyamine inhibitor-treated mice despite the warmth exposure, and there were no differences between RT and warmth-exposed, inhibitor-treated mice in any of the trabecular and cortical parameters (Figures S7A–S7F).

DISCUSSION

Over a century ago, Joel Asaph Allen proposed an ecogeographical model of adaptation to temperature differences for the homeothermic animals, in which the body surface area-to-volume ratio varies with the average temperature of the habitat, where higher temperatures would favor the higher ratios and heat dissipation, called the Allen's rule (Allen, 1877). In growing long bones, a cartilaginous disk called the growth plate separates the epiphysis from the metaphysis and diaphysis. A new cartilage is produced at the epiphyseal side of the growth plate, while the previously made cartilage at the metaphyseal side is replaced by new bone leading to bone elongation. With the onset of puberty in humans, the deposition of cartilage ceases and the metaphysis fuses with the epiphysis, leading to ceased longitudinal apposition and disappearance of the growth plate (Jilka, 2013; Pines and Hurwitz, 1991). During adulthood, bones undergo permanent remodeling that enables adaptation of the skeleton to the environment and in response to the continuous microfractures. This remodeling is kept in balance by precise coupling between the osteoclast and osteoblast activities. During aging, this exquisite balance is often disrupted, progressively leading to osteopathy. Our data show that the bone remodeling is largely affected by the environmental temperature and that warmth exposure leads to improved trabecular and cortical bone structure and strength. Interestingly, in mice while warmth exposure during development can indeed lead to lengthening of the bones (Racine et al., 2018; Serrat, 2013, 2014; Serrat et al., 2008, 2015), in our experiments applying the heat post-developmentally and during middle adulthood did not change the bone length (and thus surface area-to-volume ratio) but still increased the bone strength and mass. Accordingly, transplantation of the warm-adapted microbiota in older female and younger male

transplantation. Green shows genes with reduced or reverted expression when mice are transplanted with warm microbiota. (G) Comparison between the log fold changes of genes ($|\log_2 FC| > 1$) as in (C) using the groups of mice from (F): OvaRT versus ShamRT (red) and OvaTransp34°C versus OvaTranspRT (blue).
(H) Top 10 most deregulated reactome pathways between tibias from OvaTransp34°C and OvaTranspRT mice.
(I) Top 10 most deregulated reactome pathways between tibias from 34°C and RT mice.

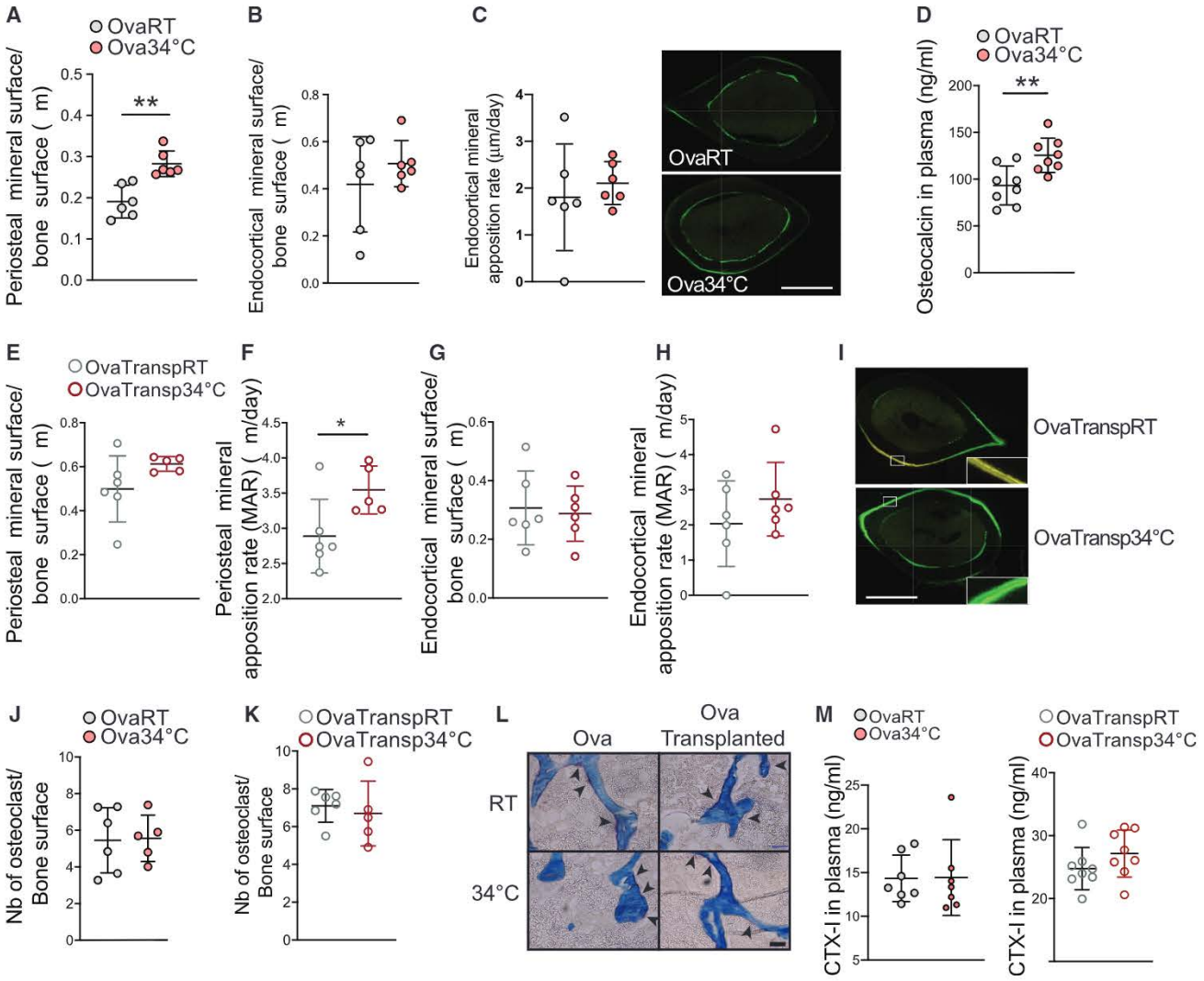

Figure 6. Warmth and Warm Microbiota Transplantation Increase Periosteal Bone Formation

(A and B) Periosteal (A) and endocortical (B) mineralized surface after calcein injection in 24-week-old female mice that were ovariectomized at 16 weeks of age and exposed for 2 months to 34°C or kept at RT.

(C) Representative images (of n = 6) of fluorescent calcein in femur midshaft used for the quantifications.

(D) Osteocalcin levels in plasma of mice as in (A).

(E–I) Periosteal mineralized surface (E), periosteal MAR (F), endocortical mineralized surface (G), and endocortical MAR (H) in tibias of 21-week-old ovariectomized, microbiota recipient female mice (OvaTransp34°C or OvaTranspRT) as in Figures 4A–4E. (I) Representative images (n = 6) of fluorescent calcein in femur midshaft used for the quantifications. Scale bar, 0.5 mm.

(J–L) TRAP staining quantification of osteoclast number in femur trabeculae of mice as in (A) shown in (J) and of mice as in (E) shown in (K). (L) Representative images (n = 6) of the quantifications shown in (J) and (K). Arrowheads correspond to the TRAP signal. Scale bar, 50 µm.

(M) CTX-1 levels in plasma of mice as in (J) and (K).

Data are shown as mean ± SD (n = 6 per group). Significance (p value) is calculated using Mann-Whitney t test, *p < 0.05; **p < 0.01; ***p < 0.001.

mice increased the bone strength and density but did not change the bone length. These data may therefore imply an extension to the Allen's rule, suggesting elongation-independent effects of warmth exposure, which predominantly favors increased bone density and strength through microbiota alterations.

The frequency of major osteoporotic fractures varies substantially depending on the country, being highest in Scandinavia and lowest in Africa. While this may partly reflect ethnic influences, it is also observed in Europe where the hip fracture rate in northern Europe is 11 times higher than in the Mediterranean area (Cheng et al., 2011; Cauley et al., 2014; Johnell et al., 1992; Eastell et al., 2016). There could be several explanations regarding the origin of these geographical differences, and it has been proposed that levels of vitamin D and calcium consumption as well as diet and genetics may be causal factors (Prentice, 2004; Yeum et al., 2016; Zengin et al., 2015). Without excluding any of the above-mentioned causes, our human metadata analysis supports a geographical gradient and shows that the osteoporosis-related hip fractures inversely correlate with the average temperatures and positively with latitude independently of

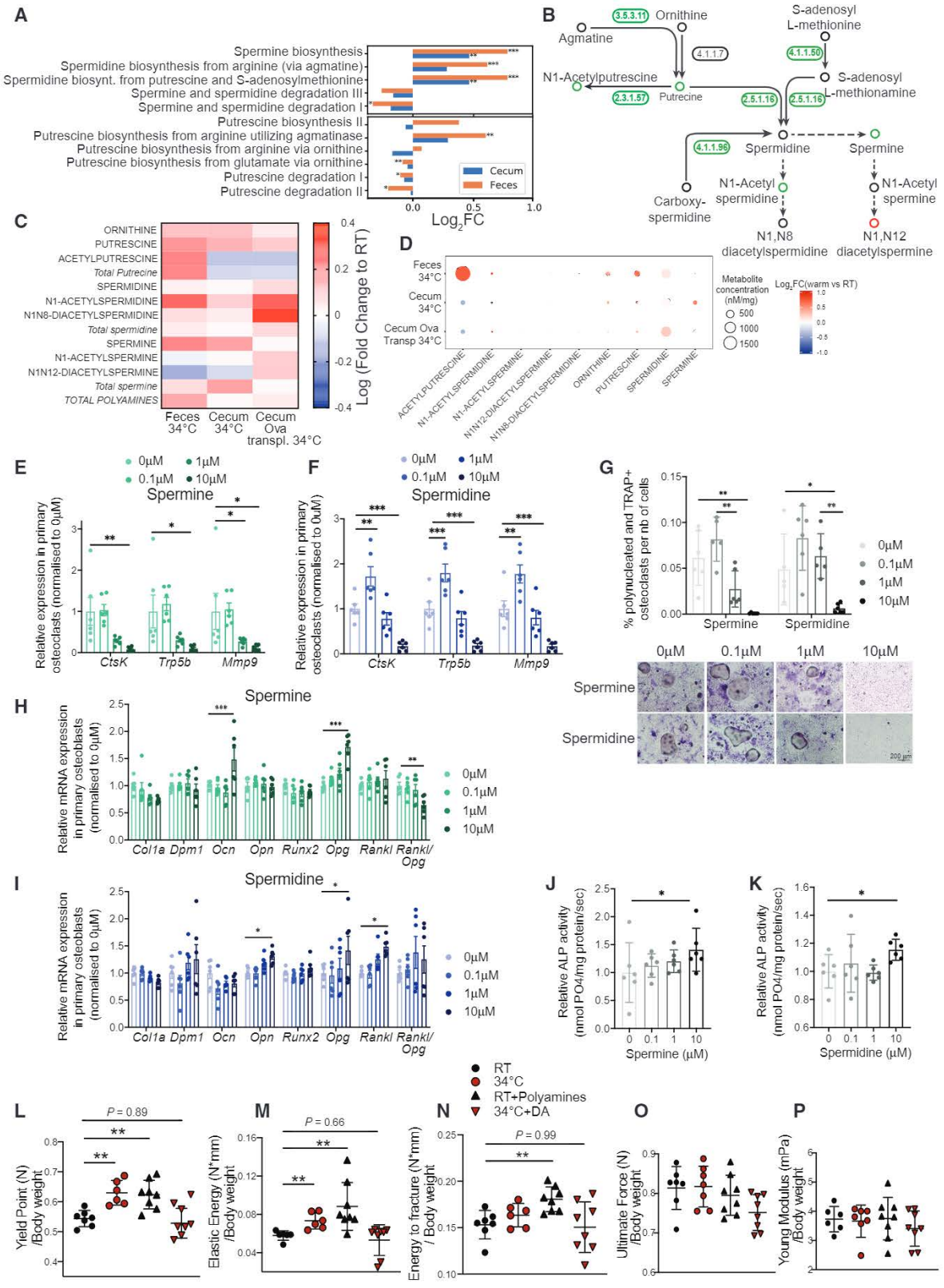

Figure 7. Microbial Production of Polyamines Mediates the Warmth Effects on the Bone

(A) Bar chart representing metagenomics analysis of the bacterial polyamine biosynthetic and degradation pathways in feces and cecum samples from 24-week-old female mice that were exposed to 34°C for 2 months or kept at RT. Significance shows FDR: *p < 0.05; **p < 0.01; ***p < 0.001.

(legend continued on next page)

vitamin D and calcium consumption, suggesting that the results we observe in mice could be translated to humans.

Our work shows that more than 90% of the ovariectomy-induced transcriptional changes in the bone are dampened by exposure to warmth and 59% by transplanting the ovariectomized mice with warm-adapted microbiota. These results suggest a major protective effect of these treatments on the overall bone alterations that underlie bone loss. The findings that the warmth exposure affects the polyamine biosynthetic pathway in the microbiota suggest a possible link between these changes and the effects on bone mass and strength and presumably other tissues that are affected by the polyamine levels. Aging is associated with decline in the polyamine levels (Scalabrino and Ferioli, 1984; Pucciarelli et al., 2012), and polyamine supplementation protects against several age-related diseases (Ramos-Molina et al., 2019; Tofalo et al., 2019), including memory impairment (Gupta et al., 2013; Frühauf et al., 2015), cardiovascular disease (Eisenberg et al., 2016), and cancer (Yue et al., 2017), while extending the lifespan of various organisms (Soda et al., 2009; Kiechl et al., 2018). Warmth-induced microbiota-mediated increases in polyamine biosynthesis may therefore be of general physiological importance that could extend well beyond bone-related research, impacting several age-related diseases and prolonging health span.

Limitations of Study

Our study does not address the upstream mechanisms by which warmth exposure alters the microbiota composition. These changes are unlikely due to a direct temperature effect as the internal body temperature of the mice was unaffected when we exposed them to 34°C. It is likely that the decreased food intake and movement during warmth exposure will jointly impact the microbiota composition to a certain extent; however, follow-up work is needed to clarify the initial triggers and pathways by which the gut microbiota responds to the increased environmental temperature. Similarly, while the study suggests a critical direct or indirect contribution of the polyamines and the gut microbiota, it does not exclude that there could be additional microbiota-related, or unrelated mechanisms by which warmth exposure increases bone strength.

STAR★METHODS

Detailed methods are provided in the online version of this paper and include the following:

- KEY RESOURCES TABLE
- RESOURCE AVAILABILITY
  - Lead Contact
  - Materials Availability
  - Data and Code Availability
- EXPERIMENTAL MODEL AND SUBJECT DETAILS
  - Mouse Models
  - Primary Cell Culture
- METHOD DETAILS
  - Ovariectomy
  - Sample Collection at Sacrifice
  - Microbiota Transplantation
  - Antibiotic Treatment
  - Polyamines Supplementation and Inhibitor Treatment
  - Micro-CT Analysis
  - Biomechanical Analysis of the Bone
  - Human Metadata Analysis
  - 16S Gut Microbiota Profiling
  - Metagenomics Sequencing
  - RNA Extraction, Reverse Transcription and Real-time qPCR
  - RNA Sequencing
  - Cecal and Fecal Concentration of Polyamines
  - Elisa
  - Bone Mineral Content
  - TRAP Staining
  - Alkaline Phosphatase (ALP) Activity Measurement
  - Bone Histomorphometric Analysis
- QUANTIFICATION AND STATISTICAL ANALYSIS
  - Data Representation and Statistical Analysis

(B) Graphical representation of the polyamine biosynthetic pathway where numbers (enzymes from keg nomenclature) represent the level of respective genes present in the gut microbiota from fecal samples of mice as in (A). Green-colored circles show increase, red-colored show decrease, and black-colored indicate unchanged concentrations after warm exposure. 3.5.3.11, agmatinase; 4.1.1.7, benzoylformate decarboxylase; 2.3.1.57, putrescine acetyltransferase/spermine-spermidine N1-acetyltransferase; 4.1.1.50, adenosylmethionine decarboxylase; 2.5.1.16, spermidine synthase; 4.1.1.96, carboxynorspermidine decarboxylase.

(C and D) Heatmap (C) or heatmap associated with absolute polyamine levels (D), showing fold change of polyamines measured using HILIC-MS/MS in feces or cecum samples from 24-week-old female mice that were exposed to 34°C for 2 months versus RT controls (34°C versus RT; feces 34°C and cecum 34°C); or cecum of 21-week-old ovariectomized, microbiota recipient female mice (cecum Ova transpl34°C).

(E and F) Relative mRNA expression levels in cultured primary osteoclasts subjected to different spermine (E) or spermidine (F) concentrations, measured by qPCR.

(G) Quantification of the polynucleated and TRAP$^+$ differentiated osteoclasts normalized to the total number of cells in presence of spermine or spermidine. Below: representative images (from 6 wells per condition) from TRAP staining of osteoclasts differentiated in presence of spermine or spermidine. Scale bar, 200 μm.

(H and I) Relative mRNA expression levels in cultured primary osteoblasts subjected to different spermine (H) or spermidine (I) concentrations, measured by qPCR.

(J and K) Relative alkaline phosphatase (ALP) activity in osteoblast culture after spermine (J) or spermidine (K) supplementation at different concentrations.

(L–P) Biomechanical analysis using three-point bending test of femur from 23-week-old female mice that were RT kept (RT), warm exposed (34°C), supplemented with freshly prepared polyamine mix and RT kept (RT-polyamines), or provided with 50 μm DA and kept at 34°C (34°C-DA), starting at 16 weeks of age until sacrifice. Polyamines and DA were supplemented in drinking water every second day. The panels show yield point (L), elastic energy (M), energy to fracture (N), ultimate force (O), and Young's modulus (P) that are normalized to their body weight values at sacrifice.

Data are shown as mean ± SD (n = 8 per group). Significance is calculated based on one-way ANOVA, *$p < 0.05$; **$p < 0.01$; ***$p < 0.001$.

Significance (p value) in all panels except (A) and (L)–(P) is calculated using Mann-Whitney t test, *$p < 0.05$; **$p < 0.01$; ***$p < 0.001$.

SUPPLEMENTAL INFORMATION

Supplemental Information can be found online at https://doi.org/10.1016/j.cmet.2020.08.012.

ACKNOWLEDGMENTS

We thank Claes Wollheim and the members of our lab for discussions and critical reading of the manuscript, and Serge Ferrari, Tony Teav, and Hector Gallart-Ayalla for technical expertise and advice. This work is part of a project that has received funding from the European Research Council (ERC) under the European Union's Horizon 2020 research and innovation program (ERC Consolidator grant agreement no. 815962, Healthybiota) and from the Clayton Foundation for biomedical research.

AUTHOR CONTRIBUTIONS

Conceptualization, C.C. and M.T.; Methodology, C.C., S.K., M.C., N.H., B.B., N.B., and M.T.; Investigation, C.C., S.K., M.C., N.H., J.B., N.S.Z., M.S., S.F., and N.B.; Writing, C.C. and M.T.; Resources, N.B., A.M., and M.T.; Funding Acquisition, M.T.; Supervision, M.T.

DECLARATION OF INTERESTS

M.T. and C.C. disclose that they are inventors of a submitted patent application for treatment of bone diseases. All other authors declare no competing interests.

Received: February 19, 2020
Revised: June 25, 2020
Accepted: August 18, 2020
Published: September 10, 2020

REFERENCES

Alhilli, F., and Wright, E.-A. (1983). The effects of changes in the environmental-temperature on the growth of tail bones in the mouse. Br. J. Exp. Pathol. *64*, 34–42.

Allen, J. (1877). The influence of physical conditions in the genesis of species. Radical Rev. *1*, 108–140.

Aramaki, T., Blanc-Mathieu, R., Endo, H., Ohkubo, K., Kanehisa, M., Goto, S., and Ogata, H. (2020). KofamKOALA: KEGG ortholog assignment based on profile HMM and adaptive score threshold. Bioinformatics *36*, 2251–2252.

Ashoub, M.A. (1958). Effect of two extreme temperatures on growth and tail-length of mice. Nature *181*, 284.

Balk, E.M., Adam, G.P., Langberg, V.N., Earley, A., Clark, P., Ebeling, P.R., Mithal, A., Rizzoli, R., Zerbini, C.A.F., Pierroz, D.D., et al. (2017). Global dietary calcium intake among adults: a systematic review. Osteoporos. Int. *28*, 3315–3324.

Boskey, A.L., and Coleman, R. (2010). Aging and bone. J. Dent. Res. *89*, 1333–1348.

Bushnell, B. (2020). BBmap. https://www.osti.gov/biblio/1241166-bbmap-fast-accurate-splice-aware-aligner.

Callahan, B.J., McMurdie, P.J., Rosen, M.J., Han, A.W., Johnson, A.J., and Holmes, S.P. (2016). DADA2: high-resolution sample inference from Illumina amplicon data. Nat. Methods *13*, 581–583.

Caporaso, J.G., Lauber, C.L., Walters, W.A., Berg-Lyons, D., Lozupone, C.A., Turnbaugh, P.J., Fierer, N., and Knight, R. (2011). Global patterns of 16S rRNA diversity at a depth of millions of sequences per sample. Proc. Natl. Acad. Sci. USA *108*, 4516–4522.

Caporaso, J.G., Lauber, C.L., Walters, W.A., Berg-Lyons, D., Huntley, J., Fierer, N., Owens, S.M., Betley, J., Fraser, L., Bauer, M., et al. (2012). Ultra-high-throughput microbial community analysis on the Illumina HiSeq and MiSeq platforms. ISME J. *6*, 1621–1624.

Caspi, R., Billington, R., Ferrer, L., Foerster, H., Fulcher, C.A., Keseler, I.M., Kothari, A., Krummenacker, M., Latendresse, M., Mueller, L.A., et al. (2016). The MetaCyc database of metabolic pathways and enzymes and the BioCyc collection of pathway/genome databases. Nucleic Acids Res. *44*, D471–D480.

Cauley, J.A., Chalhoub, D., Kassem, A.M., and El-Hajj Fuleihan, Gel-H. (2014). Geographic and ethnic disparities in osteoporotic fractures. Nat. Rev. Endocrinol. *10*, 338–351.

Cheng, S.Y., Levy, A.R., Lefaivre, K.A., Guy, P., Kuramoto, L., and Sobolev, B. (2011). Geographic trends in incidence of hip fractures: a comprehensive literature review. Osteoporos. Int. *22*, 2575–2586.

Chevalier, C., Stojanović, O., Colin, D.J., Suarez-Zamorano, N., Tarallo, V., Veyrat-Durebex, C., Rigo, D., Fabbiano, S., Stevanović, A., Hagemann, S., et al. (2015). Gut microbiota orchestrates energy homeostasis during cold. Cell *163*, 1360–1374.

Cox-York, K.A., Sheflin, A.M., Foster, M.T., Gentile, C.L., Kahl, A., Koch, L.G., Britton, S.L., and Weir, T.L. (2015). Ovariectomy results in differential shifts in gut microbiota in low versus high aerobic capacity rats. Physiol. Rep. *3*, e12488.

Demontiero, O., Vidal, C., and Duque, G. (2012). Aging and bone loss: new insights for the clinician. Ther. Adv. Musculoskelet. Dis. *4*, 61–76.

Devlin, M.J., Cloutier, A.M., Thomas, N.A., Panus, D.A., Lotinun, S., Pinz, I., Baron, R., Rosen, C.J., and Bouxsein, M.L. (2010). Caloric restriction leads to high marrow adiposity and low bone mass in growing mice. J. Bone Miner. Res. *25*, 2078–2088.

Eastell, R., O'Neill, T.W., Hofbauer, L.C., Langdahl, B., Reid, I.R., Gold, D.T., and Cummings, S.R. (2016). Postmenopausal osteoporosis. Nat. Rev. Dis. Primers *2*, 16069.

Eisenberg, T., Abdellatif, M., Schroeder, S., Primessnig, U., Stekovic, S., Pendl, T., Harger, A., Schipke, J., Zimmermann, A., Schmidt, A., et al. (2016). Cardioprotection and lifespan extension by the natural polyamine spermidine. Nat. Med. *22*, 1428–1438.

Fabbiano, S., Suárez-Zamorano, N., Rigo, D., Veyrat-Durebex, C., Stevanovic Dokic, A.S., Colin, D.J., and Trajkovski, M. (2016). Caloric restriction leads to browning of white adipose tissue through type 2 immune signaling. Cell Metab. *24*, 434–446.

Fabregat, A., Sidiropoulos, K., Viteri, G., Forner, O., Marin-Garcia, P., Arnau, V., D'Eustachio, P., Stein, L., and Hermjakob, H. (2017). Reactome pathway analysis: a high-performance in-memory approach. BMC Bioinformatics *18*, 142.

Fernandes, A.D., Macklaim, J.M., Linn, T.G., Reid, G., and Gloor, G.B. (2013). ANOVA-like differential expression (ALDEx) analysis for mixed population RNA-Seq. PLoS One *8*, e67019.

Ferris, R.L., Blumenschein, G.R., Fayette, J., Guigay, J., Colevas, A.D., Licitra, L., Harrington, K., Kasper, S., Vokes, E.E., Even, C., et al. (2018). Two-year update From CheckMate 141: outcomes with Nivolumab (Nivo) vs Investigator's choice (IC) in recurrent or metastatic (R/M) squamous cell carcinoma of the head and neck (SCCHN) in the overall population and PD-L1 subgroups. International Journal of Radiation Oncology*Biology*Physics *100*, 1317.

Frühauf, P.K., Ineu, R.P., Tomazi, L., Duarte, T., Mello, C.F., and Rubin, M.A. (2015). Spermine reverses lipopolysaccharide-induced memory deficit in mice. J. Neuroinflamm. *12*, 3.

Gupta, V.K., Scheunemann, L., Eisenberg, T., Mertel, S., Bhukel, A., Koemans, T.S., Kramer, J.M., Liu, K.S.Y., Schroeder, S., Stunnenberg, H.G., et al. (2013). Restoring polyamines protects from age-induced memory impairment in an autophagy-dependent manner. Nat. Neurosci. *16*, 1453–1460.

Hamrick, M.W., Ding, K.H., Ponnala, S., Ferrari, S.L., and Isales, C.M. (2008). Caloric restriction decreases cortical bone mass but spares trabecular bone in the mouse skeleton: implications for the regulation of bone mass by body weight. J. Bone Miner. Res. *23*, 870–878.

Harland, S.C. (1960). Effect of temperature on growth in weight and tail-length of inbred and hybrid mice. Nature *186*, 446.

Hsu, E., and Pacifici, R. (2018). From osteoimmunology to osteomicrobiology: how the microbiota and the immune system regulate bone. Calcif. Tissue Int. *102*, 512–521.

Hyatt, D., Chen, G.L., Locascio, P.F., Land, M.L., Larimer, F.W., and Hauser, L.J. (2010). Prodigal: prokaryotic gene recognition and translation initiation site identification. BMC Bioinformatics *11*, 119.

Iwaniec, U.T., Philbrick, K.A., Wong, C.P., Gordon, J.L., Kahler-Quesada, A.M., Olson, D.A., Branscum, A.J., Sargent, J.L., DeMambro, V.E., Rosen, C.J., and Turner, R.T. (2016). Room temperature housing results in premature cancellous bone loss in growing female mice: implications for the mouse as a preclinical model for age-related bone loss. Osteoporos. Int. *27*, 3091–3101.

Jilka, R.L. (2013). The relevance of mouse models for investigating age-related bone loss in humans. J. Gerontol. A Biol. Sci. Med. Sci. *68*, 1209–1217.

Johnell, O., Gullberg, B., Allander, E., and Kanis, J.A.; MEDOS Study Group. (1992). The apparent incidence of hip fracture in Europe: a study of national register sources. Osteoporos. Int. *2*, 298–302.

Jones, R.M., Mulle, J.G., and Pacifici, R. (2017). Osteomicrobiology: the influence of gut microbiota on bone in health and disease. Bone *115*, 59–67.

Kaiyala, K.J., Morton, G.J., Thaler, J.P., Meek, T.H., Tylee, T., Ogimoto, K., and Wisse, B.E. (2012). Acutely decreased thermoregulatory energy expenditure or decreased activity energy expenditure both acutely reduce food intake in mice. PLoS One *7*, e41473.

Kaliannan, K., Robertson, R.C., Murphy, K., Stanton, C., Kang, C., Wang, B., Hao, L., Bhan, A.K., and Kang, J.X. (2018). Estrogen-mediated gut microbiome alterations influence sexual dimorphism in metabolic syndrome in mice. Microbiome *6*, 205.

Kang, D.D., Li, F., Kirton, E.S., Thomas, A., Egan, R.S., An, H., and Wang, Z. (2019). MetaBAT 2: an adaptive binning algorithm for robust and efficient genome reconstruction from metagenome assemblies. PeerJ *7*, e7359.

Karvonen, E., Kauppinen, L., Partanen, T., and Pösö, H. (1985). Irreversible inhibition of putrescine-stimulated S-adenosyl-L-methionine decarboxylase by berenil and pentamidine. Biochem J. *231*, 165–169.

Kasper, S., Gillison, M.L., Blumenschein, G., Fayette, J., Guigay, J., Colevas, A.D., Licitra, L., Harrington, K., Vokes, E.E., Even, C., et al. (2018). Nivolumab (Nivo) vs Investigator's choice (IC) for platinum-refractory (PR) recurrent or metastatic (R/M) squamous cell carcinoma of the head and neck (SCCHN; CheckMate 141): outcomes in first-line (1L) R/M Patients (Pts) and updated safety and efficacy. Oncol. Res. Treat. *41*, 96.

Kiechl, S., Pechlaner, R., Willeit, P., Notdurfter, M., Paulweber, B., Willeit, K., Werner, P., Ruckenstuhl, C., Iglseder, B., Weger, S., et al. (2018). Higher spermidine intake is linked to lower mortality: a prospective population-based study. Am. J. Clin. Nutr. *108*, 371–380.

Kieser, S., Brown, J., Zdobnov, E.M., Trajkovski, M., and McCue, L.A. (2020). Atlas: a Snakemake workflow for assembly, annotation, and genomic binning of metagenome sequence data. BMC Bioinformatics *21*, 257.

Li, L., Rao, S., Cheng, Y., Zhuo, X., Deng, C., Xu, N., Zhang, H., and Yang, L. (2019). Microbial osteoporosis: the interplay between the gut microbiota and bones via host metabolism and immunity. MicrobiologyOpen *8*, e00810.

Libby, P.R., and Porter, C.W. (1992). Inhibition of enzymes of polyamine backconversion by pentamidine and berenil. Biochem Pharmacol. *44*, 830–832.

Madeira, F., Park, Y.M., Lee, J., Buso, N., Gur, T., Madhusoodanan, N., Basutkar, P., Tivey, A.R.N., Potter, S.C., Finn, R.D., and Lopez, R.D. (2019). The EMBL-EBI search and sequence analysis tools APIs in 2019. Nucleic Acids Res. *47*, W636–W641.

Markle, J.G., Frank, D.N., Mortin-Toth, S., Robertson, C.E., Feazel, L.M., Rolle-Kampczyk, U., von Bergen, M., McCoy, K.D., Macpherson, A.J., and Danska, J.S. (2013). Sex differences in the gut microbiome drive hormone-dependent regulation of autoimmunity. Science *339*, 1084–1088.

Martín-Fernández, J.A., Barcelo-Vidal, C., and Pawlowsky-Glahn, V. (2003). Dealing with zeros and missing values in compositional data sets using nonparametric imputation. Math. Geol. *35*, 253–278.

Mcmillan, P.J., Dewri, R.A., Joseph, E.E., Schultz, R.L., and Deftos, L.J. (1989). Rapid changes of light microscopic indices of osteoclast-bone relationships correlated with electron microscopy. Calcif. Tissue Int. *44*, 399–405.

Meyer, C.W., Ootsuka, Y., and Romanovsky, A.A. (2017). Body temperature measurements for metabolic phenotyping in mice. Front. Physiol. *8*, 520.

Mosekilde, L. (2000). Age-related changes in bone mass, structure, and strength - effects of loading. Z. Rheumatol. *59*, 1–9.

Neidhart, M., Karouzakis, E., Jüngel, A., Gay, R.E., and Gay, S. (2014). Inhibition of spermidine/spermine N1-acetyltransferase activity: a new therapeutic concept in rheumatoid arthritis. Arthritis Rheumatol. *66*, 1723–1733.

Nurk, S., Meleshko, D., Korobeynikov, A., and Pevzner, P.A. (2017). metaSPAdes: a new versatile metagenomic assembler. Genome Res *27*, 824–834.

Ohlsson, C., and Sjögren, K. (2015). Effects of the gut microbiota on bone mass. Trends Endocrinol. Metab. *26*, 69–74.

Ohlsson, C., and Sjögren, K. (2018). Osteomicrobiology: a new cross-disciplinary research field. Calcif. Tissue Int. *102*, 426–432.

Parfitt, A.M. (1988). Bone histomorphometry: proposed system for standardization of nomenclature, symbols, and units. Calcif. Tissue Int. *42*, 284–286.

Parks, D.H., Imelfort, M., Skennerton, C.T., Hugenholtz, P., and Tyson, G.W. (2015). CheckM: assessing the quality of microbial genomes recovered from isolates, single cells, and metagenomes. Genome Res *25*, 1043–1055.

Parvaneh, K., Jamaluddin, R., Karimi, G., and Erfani, R. (2014). Effect of probiotics supplementation on bone mineral content and bone mass density. Sci. World J. *2014*, 595962.

Pegg, A.E. (2009). Mammalian polyamine metabolism and function. IUBMB Life *61*, 880–894.

Pines, M., and Hurwitz, S. (1991). The role of the growth plate in longitudinal bone growth. Poult. Sci. *70*, 1806–1814.

Prentice, A. (2004). Diet, nutrition and the prevention of osteoporosis. Public Health Nutr. *7*, 227–243.

Pucciarelli, S., Moreschini, B., Micozzi, D., De Fronzo, G.S., Carpi, F.M., Polzonetti, V., Vincenzetti, S., Mignini, F., and Napolioni, V. (2012). Spermidine and spermine are enriched in whole blood of nona/centenarians. Rejuvenation Res. *15*, 590–595.

Quast, C., Pruesse, E., Yilmaz, P., Gerken, J., Schweer, T., Yarza, P., Peplies, J., and Glöckner, F.O. (2013). The SILVA ribosomal RNA gene database project: improved data processing and web-based tools. Nucleic Acids Res. *41*, D590–D596.

Racine, H.L., Meadows, C.A., Ion, G., and Serrat, M.A. (2018). Heat-induced limb length asymmetry has functional impact on weight bearing in mouse hindlimbs. Front. Endocrinol. *9*, 289.

Ramos-Molina, B., Queipo-Ortuño, M.I., Lambertos, A., Tinahones, F.J., and Peñafiel, R. (2019). Dietary and gut microbiota polyamines in obesity- and age-related diseases. Front. Nutr. *6*, 24.

Reginster, J.Y., and Burlet, N. (2006). Osteoporosis: a still increasing prevalence. Bone *38*, S4–S9.

Romsos, D.R., Ferguson, D., and Vander Tuig, J.G. (1985). Effects of a warm environment on energy balance in obese (Ob/Ob) mice. Metab. Clin. Exp. *34*, 931–937.

Scalabrino, G., and Ferioli, M.E. (1984). Polyamines in mammalian ageing: an oncological problem, too? A review. Mech. Ageing Dev. *26*, 149–164.

Serrat, M.A. (2013). Allen's rule revisited: temperature influences bone elongation During a critical period of postnatal development. Anat. Rec. (Hoboken) *296*, 1534–1545.

Serrat, M.A. (2014). Environmental temperature impact on bone and cartilage growth. Compr. Physiol. *4*, 621–655.

Serrat, M.A., King, D., and Lovejoy, C.O. (2008). Temperature regulates limb length in homeotherms by directly modulating cartilage growth. Proc. Natl. Acad. Sci. USA *105*, 19348–19353.

Serrat, M.A., Schlierf, T.J., Efaw, M.L., Shuler, F.D., Godby, J., Stanko, L.M., and Tamski, H.L. (2015). Unilateral heat accelerates bone elongation and lengthens extremities of growing mice. J. Orthop. Res. *33*, 692–698.

Sieber, C.M.K., Probst, A.J., Sharrar, A., Thomas, B.C., Hess, M., Tringe, S.G., and Banfield, J.F. (2018). Recovery of genomes from metagenomes via a dereplication, aggregation and scoring strategy. Nat. Microbiol. *3*, 836–843.

Sjögren, K., Engdahl, C., Henning, P., Lerner, U.H., Tremaroli, V., Lagerquist, M.K., Bäckhed, F., and Ohlsson, C. (2012). The gut microbiota regulates bone mass in mice. J. Bone Miner. Res. *27*, 1357–1367.

Skipper, S., and Perktold, J. (2010). statsmodels: econometric and statistical modeling with python. In Proceedings of the 9th python in science conference https://conference.scipy.org/proceedings/scipy2010/pdfs/seabold.pdf.

Soda, K., Dobashi, Y., Kano, Y., Tsujinaka, S., and Konishi, F. (2009). Polyamine-rich food decreases age-associated pathology and mortality in aged mice. Exp. Gerontol. *44*, 727–732.

Sözen, T., Özışık, L., and Başaran, N.Ç. (2017). An overview and management of osteoporosis. Eur. J. Rheumatol. *4*, 46–56.

Steinegger, M., and Söding, J. (2018). Clustering huge protein sequence sets in linear time. Nat. Commun. *9*, 2542.

Suárez-Zamorano, N., Fabbiano, S., Chevalier, C., Stojanović, O., Colin, D.J., Stevanović, A., Veyrat-Durebex, C., Tarallo, V., Rigo, D., Germain, S., et al. (2015). Microbiota depletion promotes browning of white adipose tissue and reduces obesity. Nat. Med. *21*, 1497–1501.

Tofalo, R., Cocchi, S., and Suzzi, G. (2019). Polyamines and gut microbiota. Front. Nutr. *6*, 16.

Tsai, Y.F., Hsu, L.H., Wu, C.C., Cai, W.H., Yang, K.C., and Fan, F.Y. (2017). Long-term oral toxicity and anti-osteoporotic effect of sintered dicalcium pyrophosphate in rat model of postmenopausal osteoporosis. J. Med. Biol. Eng. *37*, 181–190.

Wahl, D.A., Cooper, C., Ebeling, P.R., Eggersdorfer, M., Hilger, J., Hoffmann, K., Josse, R., Kanis, J.A., Mithal, A., Pierroz, D.D., et al. (2012). A global representation of vitamin D status in healthy populations. Arch. Osteoporos. *7*, 155–172.

Wang, L.L., Liu, Y., Qi, C., Shen, L.Y., Wang, J.Y., Liu, X.J., Zhang, N., Bing, T., and Shangguan, D.H. (2018). Oxidative degradation of polyamines by serum supplement causes cytotoxicity on cultured cells. Sci. Rep. *8*, 10384.

Wu, Y.W., Simmons, B.A., and Singer, S.W. (2016). MaxBin 2.0: an automated binning algorithm to recover genomes from multiple metagenomic datasets. Bioinformatics *32*, 605–607.

Yamamoto, T., Hinoi, E., Fujita, H., Iezaki, T., Takahata, Y., Takamori, M., and Yoneda, Y. (2012). The natural polyamines spermidine and spermine prevent bone loss through preferential disruption of osteoclastic activation in ovariectomized mice. Br. J. Pharmacol. *166*, 1084–1096.

Yeum, K.J., Song, B.C., and Joo, N.S. (2016). Impact of geographic location on vitamin D status and bone mineral density. Int. J. Environ. Res. Public Health *13*, 184.

Yue, F., Li, W., Zou, J., Jiang, X., Xu, G., Huang, H., and Liu, L. (2017). Spermidine prolongs lifespan and prevents liver fibrosis and hepatocellular carcinoma by activating MAP1S-mediated autophagy. Cancer Res. *77*, 2938–2951.

Zengin, A., Prentice, A., and Ward, K.A. (2015). Ethnic differences in bone health. Front. Endocrinol. (Lausanne) *6*, 24.

Ziętak, M., Kovatcheva-Datchary, P., Markiewicz, L.H., Ståhlman, M., Kozak, L.P., and Bäckhed, F. (2016). Altered microbiota contributes to reduced diet-induced obesity upon cold exposure. Cell Metab. *23*, 1216–1223.

STAR★METHODS

KEY RESOURCES TABLE

REAGENT or RESOURCE	SOURCE	IDENTIFIER
Chemicals, Peptides, and Recombinant Proteins		
Calcein	Sigma-Aldrich	C0875
RNA-later	Invitrogen	AM7020
Neomycin-streptomycin-penicillin	Sigma-Aldrich	P4083
Vancomycin	Sigma-Aldrich	V2002
Metronidazole	Sigma-Aldrich	M3761
Bacitracin	Sigma-Aldrich	11702
Ciprofloxacine HCL	Alkaloid	2000314
CEFAZ	Alkaloid	1046371
Spermine for *in vivo*	Sigma-Aldrich	85590
Spermidine for *in vivo*	Sigma-Aldrich	S2626
Diaminazene Acetureate	Sigma-Aldrich	D7770
Trizol	Thermo Fisher Scientific	15596018
High-Capacity cDNA Reverse Transcription Kit	Applied Biosystems	4368813
Power-up SYBR Green	Applied Biosystems	A25742
aMEM medium	bioconcept	1-23P10-M
100X Penicillin Streptomycin	GIBCO	15140
100x glutamine	GIBCO	25030
amino-acids mix	BioConcept	5-12K01-H
Recombinant murine M-CFS	Peprotech	31502
Recombinant murine sRANK Ligand	Peprotech	315-11C
Spermine for cell culture	Sigma-Aldrich	S4264
Spermidine for cell culture	Sigma-Aldrich	S0266
Fast violet B salt	ChemCruz	sc-215029B
Sirius red dye reagent: Direct red 80	Sigma-Aldrich	P744
Critical Commercial Assays		
PowerFecal DNA Kit	QIAGEN	12830-50
5Prime HotMaster mix	Quantabio	2200400
MiSeq reagent kit V2	Illumina	MS-102-2003
TruSeq Nano DNA Library Prep Kit	Illumina	20015964
TruSeq RNA Library Prep Kit v2	Illumina	RS-122-2001
Calcitriol (INN) Elisa kit	Abbexa	abx 513030
Osteocalcin Elisa Kit	Immutopics (quidel)	60-1305
RatLaps CTX-I EIA	Immunodiagnostic Systems	AC-06F1
Pierce BCA Protein assay kit	Thermo Scientific	23225
Deposited Data		
Raw shotgun-metagenome data of female mice	This study	PRJNA647832
Raw amplicon data of male mice	This study	PRJNA648020
Raw amplicon data of female mice	This study	PRJNA647833
Raw RNA seq data	This study	PRJNA648022
SILVA database v132	(Quast et al., 2013)	N/A
Reactome pathways database	(Fabregat et al., 2017)	N/A

(*Continued on next page*)

Continued

REAGENT or RESOURCE	SOURCE	IDENTIFIER
Resources for the metagenomic analysis	This study	https://github.com/SilasK/WarmMicrobiota
Resources for the 16SrDNA analysis	This study	https://github.com/SilasK/WarmMicrobiota
Resources for the human correlation analysis	This study	https://dx.doi.org/10.6084/m9.figshare.0.12696407
Targeted Metabolomic data	This study	https://dx.doi.org/10.6084/m9.figshare.12696419
Experimental Models: Organisms/Strains		
C57BL/6J mice	Janvier Labs	SC-C57J-M
Germ-free mice on C57BL/6J background	Germ-free Clean Animal Facility, University of Bern, Switzerland	N/A
Oligonucleotides		
Primer for 16S rDNA library preparation: 806 Reverse Primer GGACTACNVGGG TWTCTAAT - 515 Forward Primer GTG YCAGCMGCCGCGGTAA.	515F-806R barcoded primers Integrated DNA Technologies (IDT)	10776320 (plate5) and 10776323 (plate6)
Primer for 16S rDNA library sequencing: read1, 5′- TATGGTAA TTGTGTGCCAGCMGCCGCGGTA A-3′, read2, 5′- AGTCAGTCAGCCG GACTACHVGGGTWTCTAAT3′ and index read, 5′- ATTAGAWACCCBD GTAGTCCGGCTGACTGACT3′	Illumina	N/A
Primer used for the cell culture characterization: See Table S1	This study	N/A
Software and Algorithms		
VivaCT40 associated software	Scanco system; Zurich, Switzerland	N/A
Instron 1114 associated software	Instron, High Wycombe, UK	N/A
Amplicon sequencing plipline	https://github.com/SilasK/16S-dada2	N/A
Statistical 16S data analysis	https://github.com/SilasK/microbiome-analysis	N/A
Sci-kit bio, compositional data analysis	http://scikit-bio.org/	N/A
Metagenomic reads analysis: metagenome-atlas v2	(Kieser et al., 2020)	N/A
MetaCyc Pathways	(Caspi et al., 2016)	N/A
TopHat v.2 software	John Hopkins university	N/A
RSeQC V2.3.3	N/A	http://rseqc.sourceforge.net/
PicardTools1.92	N/A	https://broadinstitute.github.io/picard/
R/Bioconductor package EdgeR v.3.4.2	N/A	https://www.bioconductor.org/packages/release/bioc/html/edgeR.html
Raw LC-MS/MS data was processed using the Agilent Quantitative analysis software (version B.07.00)	MassHunter Agilent technologies	N/A
Metaexpress (5.1.41) software	Molecular devices	N/A
Leica Q image analyzer	Leica	N/A
Bioquant osteo software	Bioquant	N/A

RESOURCE AVAILABILITY

Lead Contact

Further information and requests for resources and reagents should be directed to and will be fulfilled by the Lead Contact, Mirko Trajkovski (Mirko.Trajkovski@unige.ch)

Materials Availability

All materials used in this study are either commercially available or obtained through collaboration, as indicated.

Data and Code Availability

All sequencing data generated in this study is deposited at the Sequence Read Archive (SRA) of the National Center for Biotechnology Information. The 16S rDNA sequencing of the female and the male mice have accessions SRA: PRJNA647833 and SRA: PRJNA648020, respectively. Shotgun metagenomics data is available under the id SRA: PRJNA647832 and the RNA seq data under SRA: PRJNA648022. The data for targeted metabolomics and the correlation analysis in human are deposited in the open access repository figshare: https://doi.org/10.6084/m9.figshare.12696419 and https://doi.org/10.6084/m9.figshare 0.12696407, respectively. The scripts used for the analysis of the 16S rDNA, metagenomc and human epidemiology data are available at https://github.com/SilasK/WarmMicrobiota.

EXPERIMENTAL MODEL AND SUBJECT DETAILS

Mouse Models

All C57BL/6J mice were purchased from Janvier Labs and were kept in a specific pathogen-free facility (SPF) in individually ventilated cages, 2 mice per cage. All mice were in a 12-h day/night cycle and fed a standard chow diet (SDS RN3). Upon arrival and before the start of the experiment, mice were allowed to acclimatize in the new environment for 1 week. GF mice on C57BL/6J background were obtained from the GF clean animal facility of the University of Bern (in collaboration with A.M.) and transplanted with donor microbiota immediately upon arrival. At the start of the experiments, the male mice were at 8 weeks, and females were at 16 weeks of age. Animals were equally allocated into groups based on their body weight to ensure equal starting points, and otherwise randomly. Warmth exposure was done at 34°C in a light and humidity-controlled climatic chamber (TSE, Germany) in SPF conditions using individually ventilated cages. The 34°C-like pair-fed animals were kept at room temperature (RT) and fed an equal amount to the warm exposed animals. This was equivalent to ~25% less than RT ad libitum fed, and the food was provided each day at 6pm. No signs of stress or suffering we detected in any of the mice. All animal experiments were approved by the Swiss federal and Geneva cantonal authorities for animal experimentation (Office Vétérinaire Fédéral and Commission Cantonale pour les Expériences sur les animaux de Genève).

Primary Cell Culture

Three male C57Bl/6J mice of 3 weeks old were sacrificed and their tibias, femurs and humeri were collected. After epiphyses excisions, the bone marrow was flushed, collected in αMEM 10% FBS and pooled from each bone for osteoclasts differentiation. The rest of the bone was kept for the osteoclast isolation. For the osteoclasts, after filtration through a 70 μm filter, the cells were plated in T75 in αMEM 10% FBS + 10ng/ml MCFS. After incubation for 24h at 37°C and 5% CO2, the supernatant was collected and the cells were seeded as 200 000 cells/ml in αMEM + 10% FBS + 30ng/ml MCFS. After 48h, the differentiation was initiated by adding 100ng/ml RANKL to the medium as well as spermine or spermidine at the indicated concentration (0-0.1-1-10 μM). After 14 days, RNA was extracted and cells were fixed for 1h at RT in 3.7% formaldehyde for TRAP staining. Alternatively, cells were kept in differentiating medium for 14 days and spermine and spermidine were added for 24h before RNA extraction and TRAP staining. For the osteoblasts, the bones were cut in small pieces and incubated in αMEM 10% FBS + 1mg/ml Collagenase II for 90°C at 37°C with shaking. The cells were rinsed and then incubated in αMEM10%FBS medium at 37°C with 5%CO2, and split a couple of times for proliferation before seeding them to 70 000cells/ml in differentiating medium (αMEM 10%FBS + 50μg/ml ascorbic acid + 10mM β-glycerophospate) supplemented with spermine or spermidine (at 0; 0.1; 1 and 10 μM). After 7 days of treatment, cells were harvested for RNA extraction and ALP measurements, and after 25 days of treatment for Sirius red or Alizarin red measures. The following chemical compounds were used: aMEM medium (bioconcept ref 1-23P10-M supplemented with 25mM NaHCO3, 100X Penicillin Streptomycin (Gibco Ref: 15140), 100x glutamine (Gibco Ref: 25030) and 3.75 ml amino-acids mix (BioConcept ref: 5-12K01-H)), recombinant murine M-CFS (peprotech ref 31502), recombinant murine sRANK Ligand (Peprotech ref 315-11C), Spermine (Sigma ref S4264), Spermidine (Sigma Ref: S0266).

METHOD DETAILS

Ovariectomy

Mice were anesthetized with Xylazine/Ketamine (mixture of 100 mg/kg ketamine and 16 mg/kg xylazine) and shaved below the ribs on the back side. Betadine was applied on the area for appropriate disinfection. After a 1-2 cm incision through the skin and the muscle layer just below the ribs, the ovary was localized, the fallopian tube ligated with dissolving suture and the ovary removed. The muscle layer was sutured with dissolving suture, the wound closed with staples and disinfected. The same procedure was performed on the other side. A dose of Tamgesic was administered 4 hours after the surgery, and the staples were removed 7 days after the surgery under isoflurane anesthesia. The sham-operated animals underwent the same procedure, without ligating the fallopian tube and the ovary excision.

Sample Collection at Sacrifice

To measure the dynamic indices of bone formation, mice received subcutaneous injections of calcein in saline solution at 9 and 2 days before euthanasia. 500 μl of blood was taken from terminally anesthetized mice in tubes with 10 μl of 0.5 mM EDTA, 4 μl of aprotinin (1.3%) and 4 μl of DPP-IV (10mM) and plasma stored at -80°C. Samples for RNA isolation were stored in RNAlater solution (Invitrogen ref AM7020). Bone samples for the CT-scan analysis were stored in a humid package at -20°C, and the samples for histology in 3.8% formaldehyde. All other samples snap frozen in liquid nitrogen. The tail length was measured with a ruler from the tip of the tail to the border between the fur and the skin.

Microbiota Transplantation

Upon arrival, 8 weeks old male GF mice were handled in aseptic conditions and immediately colonized by gavaging them with cecal content of the appropriate donor. The donors were male C57Bl/6J mice that were exposed to 34°C, or kept at RT for 4 weeks starting at 8 weeks of age. 500 μl of freshly collected cecal contents from donors were pooled and suspended in 5 ml of anaerobic PBS, to make a gavage mixture for each group of colonized mice. Each mouse was orally gavaged with 100 ul of the solution upon arrival and 2 days later. Animals were kept for 7 days in dirty cages from the respective donors and then switched to sterilized cages.

For microbiota transplantation of the ovariectomized mice, we used female C67Bl/6J recipients with conventional microbiota already present, and the ovariectomy was done at 16 weeks of age. The donors for these experiments were female mice that were exposed to 34°C for 4 weeks starting at 16 weeks of age. Fresh fecal pellets from the donors were freshly collected every 2 days and immediately homogenized in 1 ml of anaerobic PBS. After a short centrifugation (300g, 30sec), the supernatant was then immediately gavaged to the respective recipient. In this condition, one cage of donors (1 pellet per mouse from both mice) was used to repopulate 1 cage of recipients. Each recipient received 200 μl of the donor mixture every 2 days during 4 weeks.

Antibiotic Treatment

16-weeks-old female mice were treated with fresh antibiotics and kept at either room temperature or 34°C for 7 weeks (RT-Abx and 34°C-Abx respectively). Antibiotics cocktail was composed of 100 μg/ml neomycin, 50 μg/ml streptomycin, 100 U/ml penicillin, 50 μg/ml vancomycin, 100 μg/ml metronidazole, 100 μg/ml CEFAZ, 125 μg/ml Ciprofloxine hydrocholoride, 1 mg/ml bacitracin provided in the drinking water changed twice per week (Chevalier et al., 2015; Suárez-Zamorano et al., 2015)

Polyamines Supplementation and Inhibitor Treatment

6-weeks old C57BL/6J female mice were given a mixture of Spermine (Sigma-Aldrich) and Spermidine (Sigma-Aldrich) freshly dissolved in drinking water at concentration of 0,5mM from each compound every second day during additional 45 days at room temperature. Diaminazene Acetureate (Sigma-Aldrich) was supplemented in drinking water at a concentration of 50μM every second day during 45 days to the 16-weeks old C57BL/6J female mice that are kept at 34°C with temperature-controlled chamber in conventional facility. Food and water were given to the mice in ad libitum.

Micro-CT Analysis

The limbs were scanned in vivo before the ovariectomy to determine the basal state using a micro-CT (VivaCT40/ Scanco system; Zurich, Switzerland). After Xylazine/Ketamine anaesthesia, limb were scanned for 18 min. Final scans were performed post mortem on isolated bones. Subsequent analysis was done using micro-CT software. For the femoral and tibial trabecular region, we analyzed one hundred slices starting from 50 slices below the distal growth plate. Femoral and tibial cortical structure was assessed through 60 continuous CT slides (600 μm) from the bone midshaft. Images were segmented using an adaptative-iterative threshold approach, rather than a fixed threshold. Morphometric variables were computed from binarized images using direct 3D technique that does not rely on prior assumptions about the underlying structure (5). For trabecular bone regions, we assessed the bone volume/total volume (BV/TV). For cortical bone at the femoral and tibial midshaft, we measured the cortical bone volume (mm3) and the average cortical thickness named cortical width (μm). The lengths of the femurs were also measured from the CT-scans.

Biomechanical Analysis of the Bone

For the 3-points bending test to address the biomechanical parameters, tibias were placed on two supports separated by a distance of 9.9 mm and load was applied to the midpoint of the shaft (creating a 3-points bending). Mechanical resistance to failure (displacement and load applied) was measured using a servo-controlled electromechanical system (Instron 1114, Instron, High Wycombe, UK) with actuator displaced at 2 mm/minute. Ultimate force (maximal load, measured in Newtons [N]), Yield point (N), stiffness (elastic energy, N/mm), and energy to fracture (surface under the curve of the plastic region, N*mm) were calculated. Young's modulus (MPa) was determined by the previously described equation (Mcmillan et al., 1989).

Human Metadata Analysis

We correlated the age-standardized incidence of hip fracture (per 100'000 inhabitants) per country using the data obtained from Cauley et al. (2014) with the country's average day temperature (1961–1990, Climate Change Data, World Bank Group), or the distance from the equator (latitude) of their capitals. We accounted for the effect of calcium intake and Vitamin D serum levels (Wahl et al., 2012; Balk et al., 2017) using partial-correlation analysis. This dataset contains age-standardized incidence of hip fracture and latitude for 62 countries, temperature for 60 countries, vitamin D serum level for 38 countries and the calcium levels for 49 countries. The

regression was performed using statsmodels (Skipper and Perktold, 2010). All code is available as specified in the Key Resources Table.

16S Gut Microbiota Profiling

At the end of the experiment fecal samples were collected in sterile tubes and immediately frozen and kept at -80°C. Cecal samples were collected after sacrifice of the mice, snap frozen and conserved at -80°C. Fecal and cecal bacterial DNA was extracted using the PowerFecal DNA Kit (Qiagen, Ref. 12830-50) and the 16SrDNA library was built following the standardized protocol from the earth microbiome project (Caporaso et al., 2011, 2012). DNA was amplified with QuantaBio 5Prime HotMasterMix using barcoded universal bacterial primers targeting variable region V4 of 16SrRNA gene (515F-806R barcoded primers, Illumina): 806 Reverse Primer GGACTACNVGGGTWTCTAAT - 515 Forward Primer GTGYCAGCMGCCGCGGTAA. 2 ng of template was used and the PCR conditions included an initial denaturation at 94°C for 3', followed by 35 cycles of denaturation at 94°C for 45'', annealing at 50°C for 1', and extension at 72°C for 90'', with a final extension at 72°C for 10'. Each PCR was done in triplicates and later combined and quality checked on an agarose gel. Each PCR amplification was then quantified with Quant-iT PicoGreen dsDNA Assay with SpectraMax Gemini XPS microplate reader and pooled to an equal amount of 200 ng per sample to form the library. The library was purified using QIAquick PCR purification Kit (Qiagen, Ref. 28104), and sequenced from both ends on Illumina MiSeq (kit v2) to generate 2x250bp paired-end reads (Illumina, San Diego, CA, USA). Eighteen picometers of the library were mixed with PhiX DNA (10%) and were loaded on a MiSeq Reagent kit V2 (500 cycles) together with customized sequencing primers; read1, 5'-TATGGTAATTGTGTGC CAGCMGCCGCGGTAA-3′, read2, 5'-AGTCAGTCAGCCGGACTACHVGGGTWTCTAAT-3′ and index read, 5′-ATTAGAWACC CBDGTAGTCCGGCTGACTGACT-3′. 250 bp paired-end sequencing was performed on the MiSeq platform (Illumina, USA) in the iGE3, Institute of Genetics and Genomics in Geneva, CMU, University of Geneva. Sequencing results were obtained and de-multiplexed using standard method supplied by the MiSeq, Illumina.

Reads were processed using a pipeline based on dada2 v 1.8.0 (Callahan et al., 2016) (code accessible here : https://github.com/SilasK/16S-dada2). In short, the reads were quality filtered with the parameters (truncLen="180,100'', and maxEE=2), dereplicated, merged, and chimeras removed. sequences with length outside of 253+-7 were removed. The resulting operational taxonomic units were given numbers and were annotated with the SILVA database v132 (Quast et al., 2013). Richness and Shannon diversity were calculated after rarefaction. Compositional data analysis was performed on OTUs with at least 1 count on average using aldex2 (Fernandes et al., 2013) for the OTU, genus and family level. The reported p values are calculated using the welch test within aldex2 and were corrected for multiple testing with the Benjamini-Hochberg procedure. Principal component analysis was performed on the centered $\log_2$ ratios after multiplicative replacement of the zero values (Martín-Fernández et al., 2003).

Metagenomics Sequencing

Paired-end metagenomic libraries were prepared from 100 ngDNA using TruSeq Nano DNA Library Prep Kit (Illumina) and size selected at about 350 bp. The pooled indexed library was sequenced in a HiSeq4000 instrument at the iGE3 facility (University of Geneva).Metagenomics reads were processed using atlas v2 (Kieser et al., 2020). In short, using tools from the BBmap suite v37.78 (Bushnell, 2020), reads were quality trimmed, and contaminations from the mouse genome were filtered out. Reads were error corrected and merged before assembly with metaSpades v.1.13 (Nurk et al. 2017). Contigs were binned using metabat2 (Kang et al., 2019) and maxbin2 (Wu et al., 2016) and their predictions were combined using DAS Tool (Sieber et al., 2018). The predicted metagenome assembled genomes (MAGs), which had at least 50% completeness and < 10% contamination based on the estimation by checkM (Ferris et al., 2018; Kasper et al., 2018; Parks et al., 2015) were clustered (95% average nucleotide identity) resulting in 147 representative genomes (referred later as genomes). The genes of each genome were predicted using prodigal (Hyatt et al., 2010) and clustered using linclust (Steinegger and Söding, 2018) to a non-redundant gene catalog. The 2.3M genes were annotated using KofamScan (Aramaki et al., 2020) and InterProScan 5 (Madeira et al., 2019). Using pygenomeprop (https://github.com/Micromeda/pygenprop) the presence of genomes were annotated to contain complete or partial MetaCyc Pathways (Caspi et al., 2016). The genomes were quantified by the median of coverage in 1kb windows along the genome. MetaCyc pathways and Kegg orthologs (KO) were quantified as the sum of the relative abundance of the genomes containing them. Welch test was used for testing significant differences in pathway abundances between the groups.

RNA Extraction, Reverse Transcription and Real-time qPCR

Upon collection, tissues were stored in 1ml RNAlater and immediately processed for RNA extraction for the bone tissues or stored at -80°C. For RNA extraction, tissues were placed in 2 ml Eppendorf tubes containing 1 ml Trizol (Thermo Fisher Scientific) and mechanically disaggregated using the bead-based TissueLyser equipment (Qiagen) by shaking for 40 seconds at 30 Hz in presence of a silicate bead for the bone and a metal bead for the other tissues. After brief centrifugation to remove tissue debris (3 minutes at 12000g at 4°C), 200 µl chloroform was added, samples were shaken and centrifuged for 15 minutes at 12000g at 4°C. The chloroform phase was collected, mixed with 500 µl isopropanol and centrifuged again as before. The pellet obtained was washed twice with 70% ethanol and ultimately resuspended in 50 µl PCR-grade water. RNA from cell culture was extracted using 1ml of Trizol using the standard protocol. For retro-transcription we used High-Capacity cDNA Reverse Transcription Kit (Applied Biosystems) with 1 µg RNA per sample. qPCR were done on a LightCycler 480 machine (Roche) with SYBR Green-based detection (Applied Biosystem, Power-up). The primer sequences are shown in the Supplementary Data, as Table S1.

Results were calculated using standard curve method and normalized to the TATA box binding protein (TBP) housekeeping gene, and shown as fold change relative to the control group.

RNA Sequencing

Next Gen Sequencing of mRNA transcripts was done on Ilumina MiSeq 2500 platform at the sequencing facility of the Institute of Genetics and Genomics of Geneva (iGE3), University of Geneva. RNA was isolated from entire tibias. For the experiment comparing the ovariectomized mice transplanted with warm- or RT-microbiota (Ova. Transp. RT and Ova transp. 34°C), each group contained 4 samples where each sample correspond to one mice. For the experiment comparing Ovarectomized and sham operated mice exposed to 34°C or RT (OvaRT, Ova 34°C, shamRT and sham34°C), each group was a sample pooled from 5 mice. Libraries for the sequencing were prepared with poly-A selection according to Ilumina TrueSeq protocol. The reads were mapped with the TopHat v.2 software to the UCSC mm10 reference on new junctions and known junctions' annotations. Biological quality control and summarization were done with RSeQC-2.3.3 and PicardTools1.92.

The differential expression analysis was performed with the statistical analysis R/Bioconductor package EdgeR v.3.4.2 for the genes annotated in mm10. Briefly, the counts were normalized according to the library size and filtered. The genes above 1 count per million reads (cpm) (in experiment with replicate, in at least 3 samples) were kept for the further analysis. After normalization of the counts, transcript abundances were compared in pairwise condition in a modified Fischer exact test (as implemented in edgeR). p values of the differentially expressed genes were corrected for multiple testing error with a 5% FDR (false discovery rate), using the Benjamini-Hochberg (BH) correction. Genes were called differentially expressed between any given two conditions when their false-discovery rate was <0.05 and their fold-change >2. Transcripts with log(cpm)>0 and $p \leq 0.05$ were subsequently subjected to pathway analysis using Reactome pathways database (Fabregat et al., 2017), reporting the enrichment ratio (# DEGs/Total Genes in dataset) and FDR-adjusted pvalue computed by Fisher exact test.

Cecal and Fecal Concentration of Polyamines

Feces and cecum content samples were pre-weighed directly in the lysis tubes (soft tissue homogenizing CK 14 tubes, Bertin Technologies, Rockville, MD, US) and extracted (using ceramic beads) by adding ice-cold MeOH:H_2O (4:1; v:v) spiked with internal standards in the Cryolys Precellys 24 sample Homogenizer (2 x 20 seconds at 10000 rpm, Bertin Technologies, Rockville, MD, US). Homogenized tissue extracts were centrifuged for 15 minutes at 21000 g at 4°C and the resulting supernatant was transferred to LC-MS vials for the injection into the LC-MS system. For feces, the sample amount normalization was based on weight whereas the cecum content was extracted entirely (whole cecum per specimen). Thirteen-point calibration curves were generated by the addition of IS mixture (25 μL) to each calibrator (i.e. standard mixture) (75 μL), vortexed and transferred to LC-MS vials for the injection.

Extracted samples were analyzed by Hydrophilic Interaction Liquid Chromatography coupled to tandem mass spectrometry (HILIC - MS/MS) in positive mode using a 6495 triple quadrupole system (QqQ) interfaced with 1290 UHPLC system (Agilent Technologies). The chromatographic separation was carried out in an Acquity BEH Amide, 1.7 μm, 100 mm × 2.1 mm I.D. column (Waters, Massachusetts, US). Mobile phase was composed of A = 50 mM ammonium formate and 0.1 % FA in water and B = 50 mM ammonium formate, 0.1 % formic acid in ACN/H2O (8:2; v:v). The linear gradient elution from 100% B (0-1.5 min) down to 60% B was applied (1.5 min - 12 min) and these conditions were held for 4 min, followed by the initial chromatographic conditioning during the 5 min post-run for column re-equilibration. The flow rate was 400 μL/min, column temperature 40°C and sample injection volume 2μl. ESI source conditions were set as follows: dry gas temperature 230°C, nebulizer 35 psi and flow 14 L/min, sheath gas temperature 400°C and flow 12 L/min, nozzle voltage 500 V, and capillary voltage 4000 V. Dynamic Multiple Reaction Monitoring (dMRM) was used as acquisition mode with a total cycle time of 500 ms. Optimized collision energies for each metabolite were applied.

Raw LC-MS/MS data was processed using the Agilent Quantitative analysis software (version B.07.00, MassHunter Agilent technologies). For absolute quantification, calibration curves and the stable isotope-labeled internal standards (IS) were used to determine the response factor. Linearity of the standard curves was evaluated for each metabolite using a thirteen-point range; in addition, peak area integration was manually curated and corrected where necessary.

Elisa

1,25-dihydroxycholecalciferol was measured with Abbexa Calcitriol (INN) Elisa kit (ref: abx 513030) in 1:10 diluted plasma samples. Osteocalcin was measured with Immutopics (quidel) Elisa KIT ref 60-1305 in 1:11 diluted plasma samples. CTX-I was measured with RatLaps CTX-I EIA Immunodiagnostic Systems (ref: AC-06F1) from undiluted plasma samples. All measures were done according to manufacturers' instructions.

Bone Mineral Content

Tibias were dried in oven for 3 days at 60°C. The dry weight of each bone was recorded (w_i) and the tibias were burned and reduced to ashes with a furnace set at 800°C for 1h. The weight of the remaining ashes was measured (w_f), and the ratio between the weight of the bone ash and the dry weight (w_f/w_i) was calculated to determine the bone mineral content (Tsai et al., 2017)

TRAP Staining

Cells were fixed with 3.7% Formol (formaldehyde) for 1h at RT and rinsed with water. The staining solution was freshly prepared by mixing equal amount of Fast violet B salt (ChemCruz ref sc-215029B) solution in acetate buffer (7mg/ml), and Naphtol AS-TR phos-

phate disodium salt (Sigma ref: N6125) solution in acetate buffer (2mg/ml, 225mM sodium acetate, 75mM acetic acid and 4mM NaOH). Cells were incubated overnight at 4°C with the staining solution, rinsed with water, incubated 30 min at RT in Sodium Fluorine (4.2g/L H2O). and rinsed with water once again before being processed for imaging and analysis. Images were acquired with ZeissAxio Observer ZI and ImagexpressXL (Molecular devices). The total cells per well were quantified with Metaexpress (5.1.41) software, and the number of differentiated osteoclasts manually (defined as multinucleated and $TRAP^+$ cells).

Alkaline Phosphatase (ALP) Activity Measurement

Cells were rinsed with cold PBS and scraped in 500µl H2O. After short sonication (2x15sec-10kHtz), samples were centrifuged at 10 000rpm for 15min at 4°C. 100µl of the supernatant was collected and incubated for 10min at 37°C, while the rest of the supernatant was kept for measuring the protein concentration. The reactive solution was as the following: 10mM p-nitrophenylphosphate, 560mM 2-amino-2-methyl-1-propanol, 1mM MgCl2, pH 10.5. 900µl of the reactive solution was added to the pre-heated 100ul sample and time monitored until sample turned yellow (approx. 7min). The reaction was stopped with 200ul of 1M NaOH and the time recorded. Absorbance of the sample was measured at 405nm, and the concentration of the remaining protein was measured using Pierce BCA Protein assay kit (Thermo scientific ref 23225). The ALP activity was obtained with the following formula: ALP activity (nmol PO4/mg of prot/sec) = [(OD x 1000)/ time(sec)]/protein (mg/ml).

Bone Histomorphometric Analysis

After 24 hours of fixation in 3.8% Formol, bones were dehydrated in absolute ethanol for 3 days followed by overnight incubation in acetone at -20°C before being embedded in methyl-methacrylate (Merck). 8µm thick transversal sections of the midshaft, and sagittal section of the proximal femur were cut with Leica RM 22 65 microtome (Leica Corp Microsystems AG) and mounted unstained for the evaluation of fluorescence from the calcein deposition. Histomorphometric measurements were performed on the secondary spongiosa of the proximal tibia metaphysis and on the endocortical and periosteal bone surfaces in the middle of the tibia using Leica Q image analyzer (Leica) at 40x magnification, and Bioquant osteo software. All parameters were calculated and expressed according to standard formulas and nomenclatures (Parfitt, 1988): mineral apposition rate (micrometers per day), mineralizing surface per bone surface (percentage) and bone formation rate (cubic micrometers per square micrometer per day). Osteoclast surface per bone surface and numbers were evaluated after TRAP staining performed following the same protocol as for the cell culture staining on free floating slides and followed by a Methylene blue counterstaining and mounted with Permount (fisher chemical ref: SP15-100). Sirius red staining was performed with Sirius red dye reagent (Direct red 80 Sigma #P744, in saturated aqueous picric acid (1.3% in H2O) at concentration of 0.1% w/v).

QUANTIFICATION AND STATISTICAL ANALYSIS

Data Representation and Statistical Analysis

Plots include each datapoint, mean and ± Standard deviation (SD). All p values, n (number of animals) and each applied statistical test is specified in the figure legends. To compare two different groups we applied Mann-Whitney t test. To compare more than two groups we applied One-Way ANOVA with Tukey's multiple comparison test. All experiments were reproduced at least twice, and shown are the representative data. *In vivo* measurements were done without blinding, while the histomorphometric and biomechanical measurements were done with blinding. No data were excluded from the analysis. Where available, group sizes were calculated based on power calculations of 0.8. Results were considered significant when $p < 0.05$ in the respected statistical test and represented significance as *p <0.05; **p <0.01; ***p <0.001.

We analyzed the data using Prizm Version 8.4.3., and assembled the figures in Adobe Illustrator. We generated the graphical abstract in Powerpoint, using some of the illustrations available at Servier Medical Art.